UNIVERSITY OF OKLAHOMA

GRADUATE COLLEGE

DEVELOPMENT OF UNCONVENTIONAL RESERVOIRS: FLUID CHARACTERIZATION, STIMULATED RESERVOIR VOLUME DETERMINATION, AND PRODUCTION FORECASTING IN THE STACK

A THESIS

SUBMITTED TO THE GRADUATE FACULTY

in partial fulfillment of the requirements for the

Degree of

MASTER OF SCIENCE

By

BRADLEY R. CRONK
Norman, Oklahoma
2018

DEVELOPMENT OF UNCONVENTIONAL RESERVOIRS: FLUID CHARACTERIZATION, STIMULATED RESERVOIR VOLUME DETERMINATION, AND PRODUCTION FORECASTING IN THE STACK

A THESIS APPROVED FOR THE
MEWBOURNE SCHOOL OF PETROLEUM AND GEOLOGICAL ENGINEERING

BY

Dr. Zulfiquar Reza, Chair

Dr. Matthew Pranter

Dr. Deepak Devegowda

Acknowledgements

I feel incredibly honored to have completed my studies at the University of Oklahoma. In my time here, there have been a countless number of people behind any amount of success I have accomplished, and I will take this opportunity to thank a few of them. First, my most sincere thanks to my advisor, Dr. Zulfiquar Reza. His endless support, advisement, and encouragement throughout my graduate studies has been invaluable. I consider myself blessed to have studied with him. Along with Dr. Reza, I would also like to thank Dr. Matthew Pranter and Dr. Deepak Devegowda for serving on my committee and providing feedback on my work and thesis.

I would also like to thank my many colleagues and collaborators who have contributed a great deal to this work. First a tremendous thanks to Garrett Hickman and Joshua Miller, who contributed on the geologic aspects of this work; without their contributions, this thesis would not have been possible. A thanks to Maulin Gogri and Josue Ortiz who have collaborated on some of the engineering aspects of this thesis. I would also like to thank Dr. Andrew Cullen, Sumeer Kalra, and Warwick Energy for providing their vast knowledge and industry expertise as well as much of the data necessary to the completion of this work. Throughout this work, I will often use ‘I’, but it should be noted that the bulk of this work was completed in collaborative and integrated manner thanks to the many people listed above.

Further, I would like to thank my family. My wife, Kari, has tirelessly motivated and supported me, and I’m forever thankful for her. My parents, Trent and Delyn, have gone above and beyond in their support and encouragement of me, and there is no way I could ever thank them enough. I would also like to thank my siblings, Courtney and

Caleb, for checking in on me and always being around for dinner or to just spend time together.

Table of Contents

List of Tables

List of Figures

Abstract

The Mississippian-age Meramec Series is one of the primary producing intervals of the Sooner Trend in the Anadarko Basin of Canadian and Kingfisher (STACK) counties, Oklahoma and is currently among the most sought-after hydrocarbon plays in the US. It is a low permeability and low porosity play; therefore, an understanding of reservoir limits, fluid and petrophysical characterization, stimulated reservoir volume (SRV), and expected recovery is critical to the development planning of these reservoirs. This thesis will integrate many different engineering concepts in order address all of these crucial points of understanding.

In this thesis, first I establish an integrated workflow for multi-component fluid characterization, stimulation region limits and hydraulic fracture dimension estimation and apply the workflow to a study area of the Meramec interval in the STACK play of Oklahoma. Rate transient analysis (RTA) is used to characterize porosity, permeability, fracture dimensions and drainage areas. Subsequently, an Equation-of-State (EOS) model is established for the study area spanning the liquids-rich zone to high Gas-Oil Ratio (GOR) region. The EOS model is refined via compositional reservoir simulation by matching initial producing GORs field-wide and imposing compositional variations that would be observed due to thermal maturity. Reservoir parameters are then refined using the enhanced fluid model, and the integrated workflow is repeated until convergence.

From there, I zoom into a single well and utilize a history matching process with the use of flow simulation to understand the extent of the SRV. Within this workflow, a dual porosity model is utilized. Initially, a very large fracture network is created and the

injection of fracturing fluid is history matched. From the results of stress changes from this history matched model, the SRV is extracted. This region then becomes the only region with enhanced fracture properties, and the model is history matched again. These results generate an understanding of how the SRV is affected by hydraulic fracturing.

Then I introduce an adaption of the modified Hall Analysis that allows for very quick diagnosis of fracture efficiency. It is found that from certain properties of the introduced dHI (derivative of the Hall Integral) plot, a qualitative understanding of total fracture area and volume can be obtained. I'll also show a couple sample applications of the methodology go show how it can potentially be used.

Finally, with the model used to in history matching of the injection of hydraulic fracturing fluid, initial production is history matched. From the results of this history match, I gain an even better understanding of the enhanced properties of the SRV. This history matched model is then utilized in forecasting efforts in an attempt to understand just how much hydrocarbon can potentially be recovered from the area.

Chapter 1: Introduction and Motivation

The Mississippian-age Meramec and Osage series and the Devonian age Woodford shale are primary producing intervals of the Sooner Trend in the Anadarko Basin of Canadian and Kingfisher counties (STACK) play in central Oklahoma. Mississippian strata of the Mid-continent in north-central Oklahoma and Kansas are primarily carbonate ramp deposits. (Mazzulo, 2016) The Meramec and Osage series in central Oklahoma are the basinward equivalent of those shelf deposits and are some of the most prolific unconventional hydrocarbon reservoirs in the Mid-continent. Within the last several years, the STACK has seen rapid development as it has quickly become one of the most prolific tight oil plays in the United States. However, at the beginning of this study, very few studies had been published on the play. The ultimate goal of this thesis (alongside partner geologic studies and theses) is to further understanding in academia and industry of the play and its components.

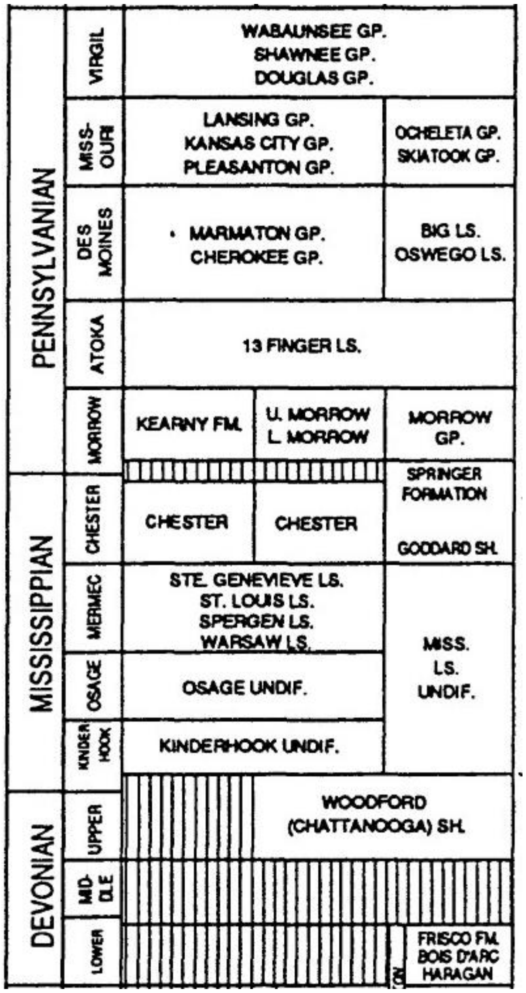

Figure 1–Chronostratigraphy of the Anadarko basin, taken from Abdallah's (2016) edit of Ball et al. (1991).

Within this play are several development targets (chronostratigraphy shown in Figure 1), but this thesis will focus on the Meramec group. The dataset used throughout this work consists of 20 wells with daily production data, daily casing and tubing pressures, public completion reports, and some completion volumes. The study area spans 1,000 mi^2 in Kingfisher, Blaine, and Canadian counties of Oklahoma. The area around and including the study area has historically been productive, allowing for relatively good control in the creation of geologic models. In this area, the Meramec is dipping from northeast to southwest with a depth ranging from 6,500 to 12,500 ft. Across this range, the reservoir spans fluid types from black oil in the shallowest zones to a condensate gas in the deepest zones studied. Figure 2 shows the location of the wells and the structure of the Meramec within the study area.

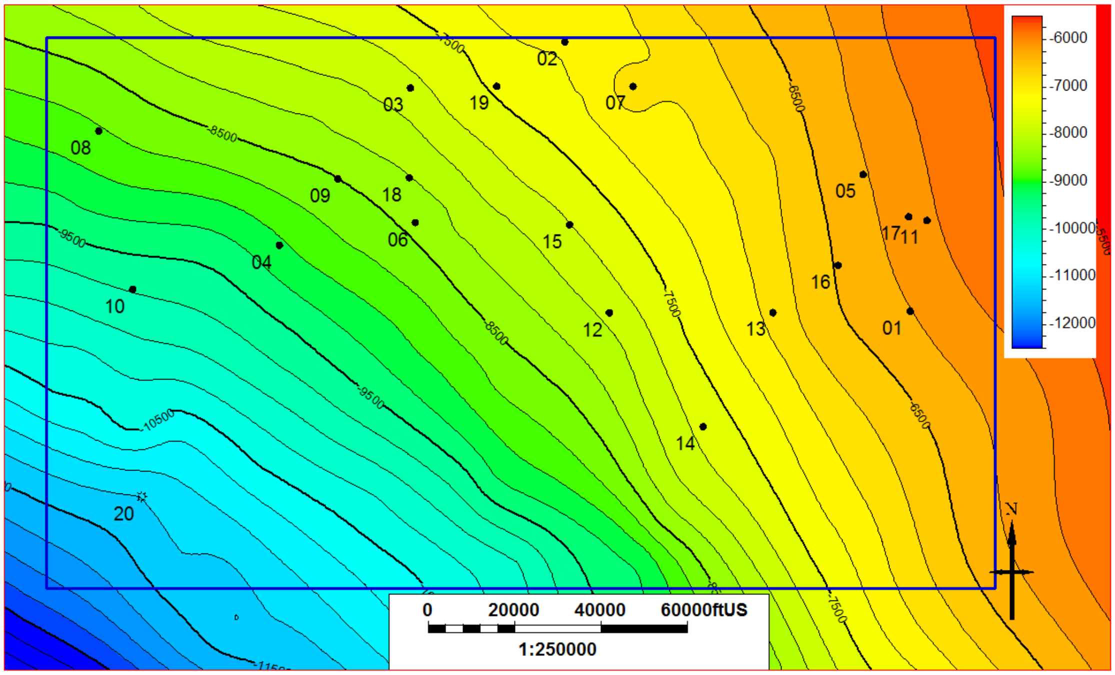

Figure 2–Map view of study area with location of wells labeled and overlain on a Meramec structure map.

In Chapter 2 of this thesis, I will review and discuss published literature that relates to the work to follow. In Chapter 3, I present an iterative workflow that allows for simultaneous solution of a unified fluid characterization, petrophysical characterization, and fracture parameters. The workflow is applied to the study area, and I provide some additional sources that give some independent validation of the results of the workflow. In Chapter 4, I discuss the modeling of hydraulic fracturing of one well in the study area. This modeling is carried out using two methods (through the use of a flow simulator and using a finite volume fracture simulator) and the results are compared. In Chapter 5, I introduce a quick approach to diagnosing fracture efficiency. The methodology adapts the Modified Hall Analysis often used in injection well diagnostics so that it can be applied to quickly diagnose key fracture parameters qualitatively. I also show a couple sample applications of the methodology. In Chapter 6, I history match production for the well referenced in Chapter 4, and work to forecast recovery from that well, and the Meramec in general. In the final two chapters, I will discuss some of the results and limitations of the results and methods in this thesis and conclude the thesis and make some recommendations for possible future studies extending from this thesis.

Chapter 2: Review of Relevant Literature

The Mississippian-age Meramec Series is one of the most productive intervals within the STACK play and has seen rapid development in recent years. It is a mixed carbonate-siliciclastic system with ultra-low permeability and porosity (Flinton 2016). It is overlain by the Chester Formation and lies on the Osage, Kinderhook, and Woodford Formations (Abdallah 2016). The fluid distribution appears to be similar to what would be seen in an unconventional, self-sourcing system, with an oil window up-dip from the gas window. Initial producing gas-oil ratios can range from below 1.0 MSCF/STB shallow in the basin to well above 1,000 MSCF/STB deeper in the basin. To date, the hydrocarbon is thought to be primarily sourced by the underlying Woodford Formation (Kornacki 2016) with some authors (Abdallah 2016) suggesting a contribution from organic rich zones in the Meramec or additional charging of hydrocarbon (Kornacki 2016).

Jones (2014) presented a methodology and field examples for extracting initial reservoir pressure from early-time flowback data. First, flowing bottomhole pressures (p_{wf}) were calculated. Then, the effect of charging from the completion was accounted for by selecting the initial reservoir pressure as the p_{wf} where first hydrocarbon production occurs. Jones also observed that this often corresponded with a plateau in pwf. Low productivity, artificial lift, and extended post-stimulation shut-in times were mentioned as potential sources of error in this methodology.

Again, using data from the STACK, Jones (2016) used reservoir simulation along with real data to describe four stages of gas-oil ratio (GOR) behavior that can be exhibited by tight oil formations. The four stages described by Jones are an initial period where GOR is equal to solution GOR, an increase in GOR after p_{wf} declines below bubblepoint pressure (p_b), a transient plateau in GOR during formation linear flow, and an increasing GOR during boundary dominated flow. Jones pointed out that all four stages will not be observed in all wells and there are several factors that will contribute to which stages are observed. Some of these factors are fracture conductivity, irreducible gas saturation, and the rate at which bottomhole pressure declines. The wells in our study exhibit similar behavior as described by Jones, and we have utilized this behavior to aid in our characterization.

Welker et al. (2016) performed trapped fluid analysis on several wells within the STACK and SCOOP. Their results indicated a decoupled gas and liquid, indicating that the hydrocarbons in the two basins were likely sourced from an oil-prone kerogen and/or had a multi-charging history. Further, they found results that could indicate generation of hydrocarbons from a single source. A liquids floor was determined to be at roughly 12,000 ft, with some exceptions.

Karacaer, Thompson, and Firincioglu (2015) developed an iterative method to determine liquid yields in the Woodford. In their study, first, an EOS was tuned using recombined fluid samples, and constant volume depletion (CVD) experiments were simulated. If these experiments did not match the observed data, the EOS was re-tuned. This EOS was then used to simulate initial producing oil yield. If needed, the recombination ratios were modified and the process is iterated to convergence. The study presented in Chapter 3 uses a methodology similar to the workflow they described.

Numerous studies over the years have found that permeability is exponentially dependent on confining stress. Bhandari et al. (2015) show an exponential relationship between permeability and confining stress in Barnett Shale cores. Katsuki et al. (2013) found a similar relationship on gas and oil shale. Their results indicate two separate exponential relationships, one above and one below pore collapse stress. Akai et al. (2016) show an exponential relationship between permeability and effective confining pressure in Montney tight gas siltstone cores; they use this relationship to evaluate the dependence of gas recovery on this relationship.

Alt II and Zoback (2017) studied the in-situ stresses and faulting in Oklahoma. Their results show that in central Oklahoma (particularly in the study area of this thesis) the maximum horizontal stress is roughly N90°E. This becomes especially relevant in Chapter 4 of this thesis, when induced hydraulic fractures are studied.

In the past several years there have been many publications seeking to model hydraulic fracturing using coupled geomechanics and fluid-flow simulators. Chin et al. (2000) use coupled simulation as a tool to understand pressure-transient problems in stress sensitive reservoirs. Ji et al. (2009) simulate hydraulic fracturing through coupling a geomechanics finite element model with a fluid flow finite difference model. This is done in an iterative method between the geomechanics grid and the flow grid, and their model is able to model the actual propagation of the fractures. Dean and Schmidt (2008) coupled a simulator that can handle hydraulic fracture growth, multiphase non-Darcy flow, as well as many other complexities and used it to predict hydraulic fracture propagation. These publications relate loosely to work in Chapter 4, although the work in this thesis uses simplified models and methods compared to coupled simulation.

Chapter 3: Integrated Fluid Characterization

A complete and accurate fluid characterization is essential to understanding a reservoir and is often one of the first tasks completed by reservoir engineers when entering a new play or embarking on simulation studies. Capturing fluid behavior allows for more accurate prediction of hydrocarbon in place, as it allows for estimation of formation volume factors and solution gas-oil ratios. Traditionally, fluid characterization requires in-depth pressure-volume-temperature (PVT) data and studies, which can be expensive and difficult to acquire. This is especially true for non-operating participants in a play, as they often do not have access to the necessary PVT information to complete fluid characterization using traditional methods. However, often times they do have access to production volumes and pressures. Given enough well control, this study utilizes the available production data to attain a representative Equation-of-State (EOS), as well as petrophysical and completion parameters.

3.1 Methodology

Two of the procedures most often initially performed when embarking on a reservoir study are fluid characterization and RTA. Both analyses require some high-quality, and often expensive data (i.e. bottomhole pressure measurements, PVT reports). Therefore, performing these analyses in absence of that data requires the engineer to make some sizable assumptions. Further complicating the issue is the interdependence of the parameters used in these two analyses. RTA requires fluid viscosities, compressibilities, and formation volume factors, as well as bottomhole pressures. A fluid characterization requires knowledge of the initial reservoir pressure. Thankfully, this study has found that this interdependence can be leveraged to benefit the engineer through use of the iterative method presented herein. The theory behind the method is that starting with some suitable analog fluid model allows for calculation of bottomhole pressures (given a wellbore schematic). Those calculated pressures can be used in rate transient analysis which will yield an estimation of the initial reservoir pressure for each well in the study. This pressure distribution can then be input into a reservoir simulator and regression of a fluid model can be performed such that initial producing gas-oil ratios are matched. This new fluid model can then be used to improve the calculation of bottomhole pressures. At this point, the process is a closed loop and can be iterated until convergence.

This study presents an iterative method, outlined in Figure 3, which allows for a full Equation-of-State (EOS) calibration across the field. First, a compositional fluid model is generated using defaults provided in commercial software. Then bottomhole pressures are calculated using this initial fluid model, production data, and simplified wellbore schematics. Initial reservoir pressure distribution is taken from initial pressures interpreted from these calculated bottomhole pressures and RTA. This pressure distribution and the initial EOS are input to a regional-scale reservoir model that consists of a porosity-permeability model for the Meremec zone. The reservoir model is initialized and flow simulation is run for some initial time period, usually one month, to capture the initial producing fluid properties. Initial producing gas-oil ratios are matched through two primary methods: imposing compositional gradients on the model and tuning the EOS parameters. Once a satisfactory match is attained, the new fluid model is used to calculate new bottomhole pressures, and the process is iterated until the fluid model reaches convergence.

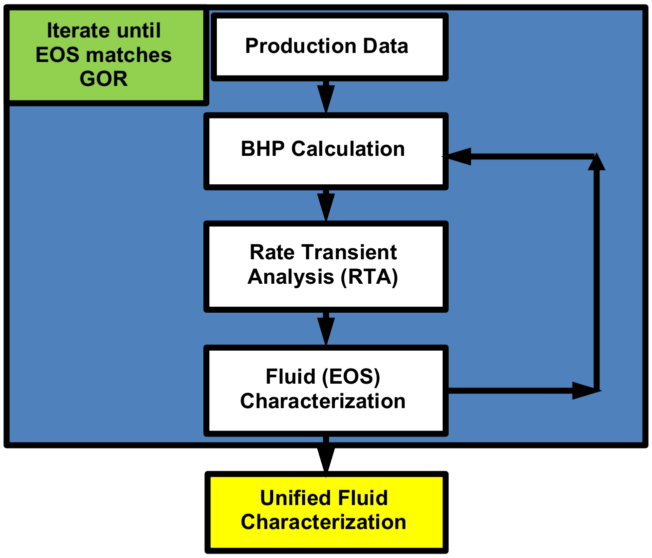

Figure 3–Schematic of workflow presented in this study.

3.1.1 Calculation of Bottomhole Pressures

Bottomhole pressures are calculated using derived vertical flow performance (VFP) tables, production rates, and tubinghead pressures. A simple L-shaped wellbore is used as input. The dimensions are taken from public completion reports available through Oklahoma Corporation Commission (2017). Reported true vertical depth (TVD) is used as the depth of the lateral section of the wellbore and reported perforation length is used as the lateral length of the wellbore. Casing dimensions are taken from the report and tubing dimensions are assumed based on the casing size (i.e. tubing size is constrained to sizes that could physically fit inside the given casing). Tubing is assumed to only be present in the vertical section of the wellbore. The temperature function used throughout the model is also used as an input and is derived from well log bottomhole temperatures in the area. Further, flow simulation is run to obtain the initial molar composition of the fluid, and this, along with the current EOS is used to develop the VFP tables.

Several wells in the dataset do not report tubing pressures for some time after initial flowback. For the purposes of this study, it is assumed that when there is no reported tubing pressure, tubing has not been installed. This is found to be a probable assumption, as evidenced by Figure 4. In this example, the assumption of flow up casing for initial time appears to hold true, as this assumption yields a smooth trend in the flowing bottomhole pressure once the calculated pressures from both wellbore schematics are combined.

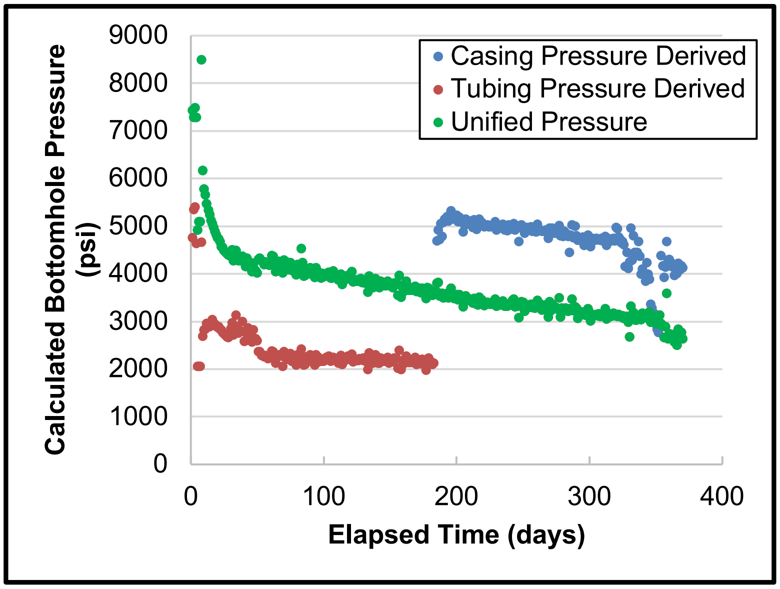

Figure 4–Bottomhole pressures for Well-04. The smooth transition in the unified bottomhole pressures serves as validation for the recombination methodology.

3.1.2 Rate Transient Analysis

RTA is carried out using a commercial software. For all wells, a fractured horizontal well model with a rectangular boundary is used. From analysis of rate-material balance time plots (sample plot provided in Figure 5), it is found that roughly half the wells in the study have attained boundary dominated flow, as tabulated in Table 1. Two reservoir models are utilized in RTA. The first is a homogeneous model. Despite several wells having exited transient flow, much of their production history comes from the transient state; therefore, the second reservoir model utilized is a dual-porosity transient slab model. As discussed later, this permits estimation of uncertainty.

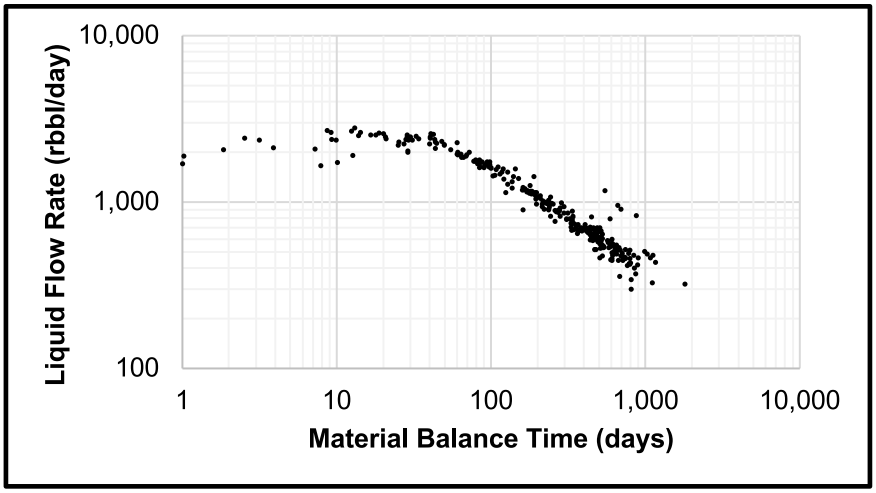

Figure 5–Sample plot used for interpretation of flow regime. If unit slope is observed, the well is interpreted to be in boundary dominated flow.

Well	Flow Regime	Well	Flow Regime
Well-01	BDF	Well-11	BDF
Well-02	BDF	Well-12	Linear
Well-03	BDF	Well-13	BDF
Well-04	Linear	Well-14	Linear
Well-05	Linear	Well-15	BDF
Well-06	Linear	Well-16	BDF
Well-07	Linear	Well-17	BDF
Well-08	BDF	Well-18	Linear
Well-09	Linear	Well-19	Linear
Well-10	Linear	Well-20	Linear

Table 1–Tabulation of flow regimes for study wells.

Calculated bottomhole flowing pressures are used as the pressure input to RTA. Downhole liquid rates are calculated using **Eq. 1** and used as the rate input; this equation is modified from that presented by Uzun et al. (2016). Implicit in this methodology is the assumption that no free gas is produced from the reservoir (all produced gas comes out of solution in the wellbore). Further, the permeability determined by RTA will be a sum of the effective oil and effective water permeability values rather than a true permeability.

$$q_l = q_{o\_surf} \cdot B_o + q_{w_{surf}} \cdot B_w \text{ ,} \qquad (1)$$

Due to the large number of unknown parameters, several reservoir parameters are used as regression variables. Bounds are placed on these parameters using general knowledge of operator design and formation reservoir properties. Table 2 outlines the regression parameters, as well as their upper and lower bounds. For some wells, the number of stages used in hydraulic fracturing is known. Senters et al. (2016) found that operators have trouble isolating stages in the STACK, so where stage information is available, it is used as an upper bound and the number of fractures is still included as a regression parameter.

	Minimum	**Maximum**
Number of Fractures	15	60[1]
Fracture Half-length, ft	50	800
Fracture Height, ft	30	300
Permeability, md	-	-
Zone Thickness, ft	60	300
Porosity, %	4	8
k_z/k_r	-	1
South Boundary, ft	x_f	800
East Boundary, ft	1/2 of well length	6,000
North Boundary, ft	x_f	800
West Boundary, ft	1/2 of well length	6,000
Drainage Area, acres	-	440

1 – Unless design is known.

Table 2– RTA regression parameters and bounds.

3.1.3 History Matching of Initial Producing GOR

The primary method used to match initial producing GOR is incorporation of compositional gradients on the fluid model. We have utilized a composition presented by Whitson (2012) as an initial starting point. Another option for history matching initial fluid properties would be to create different fluid models at different depths in the reservoir. As previously mentioned, it is believed that the oil in the region has a similar source. That being the case, the fluid should have similar Equation-of-State (EOS) properties, which would imply that observed differences in fluid behavior can be attributed to compositional gradients. Matching the fluid properties through use of compositional gradients has the unique advantage of allowing the same EOS to characterize the entire region. To further tune the fluid model in later iterations, the EOS parameters, primarily critical temperatures and pressures of plus fraction components, can be used as regression parameters to attain a better match to initial fluid behavior. We have used the EOS developed by Peng and Robinson (1976), but in practice any valid EOS could be utilized in the workflow.

3.1.4 Overpressure Hypotheses

Early in the implementation of the workflow, it was found that the pressure gradients within the study area are too high to be described by a model of a single hydraulically connected reservoir in thermodynamic equilibrium. We present some hypotheses that can match this pressure distribution, one where the reservoir is modeled using a single connected reservoir that is not in equilibrium, and three hypotheses where the reservoir is compartmentalized by baffles.

3.1.5 Uncertainty Characterization

The development of different hypotheses allows for a suite of values to be calculated. Further, different reservoir models are used in RTA to generate more possible results. Having these different results allows for an understanding of the uncertainty of the completed workflow.

3.2 Results

In this section, I present some of the key outputs of the workflow. After presenting results, I seek to provide independent validation of the values resulting from the workflow. This exercise serves to not only validate the results we are presenting, but to give credence to the workflow itself.

As mentioned previously, it was found within the interval, there are pressure gradients that cannot be explained by a single reservoir model in thermodynamic equilibrium. In order to honor the observed initial pressures, we investigated four different hypotheses that can match the observed pressures. The models are as follows (Figure 6 illustrates cases 1-3):

1. A reservoir with baffles separated by 1,000 feet vertically.
2. A reservoir with baffles oriented with suspected clinoforms.
3. A reservoir with baffles separated by 500 feet vertically.
4. A reservoir that is not in thermodynamic equilibrium (saturations, pressures, and temperatures are explicitly defined).

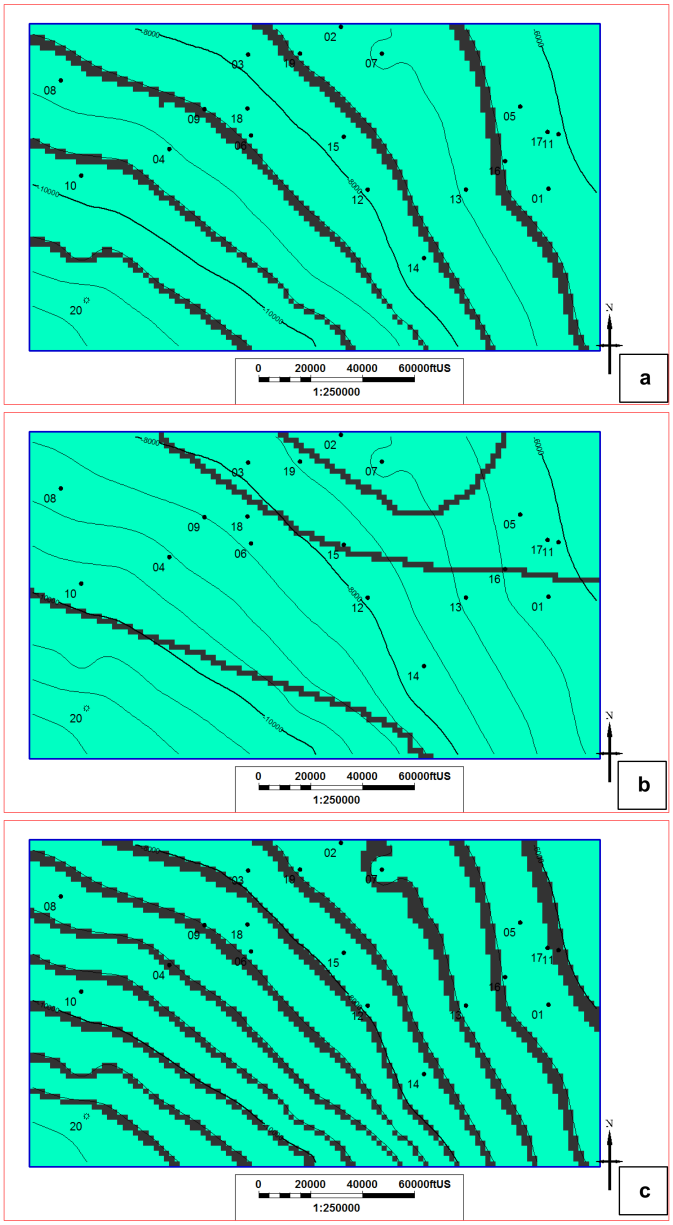

Figure 6–Location of baffles for case 1-3, (a)-(c) respectively.

Within each iteration, initial reservoir pressures are interpreted from either RTA or extrapolation of bottomhole pressures (Jones 2014). Figure 7a shows a plot of initial reservoir pressure, as found from this study, versus TVD. Also shown are the average and range of initial shut-in pressures (ISIP) taken from completion reports. While ISIP will be impacted by more than simply the reservoir pressure, the similarity in trends between the observed initial pressure and ISIP gives some validation to the observed pressures. Figure 7b is a crossplot of initial reservoir pressure and ISIP, again showing a relationship between the values. The relationship found between initial pressure and depth was used to initialize the different models. Initial pressure for the different hypotheses is shown in Figure 8.

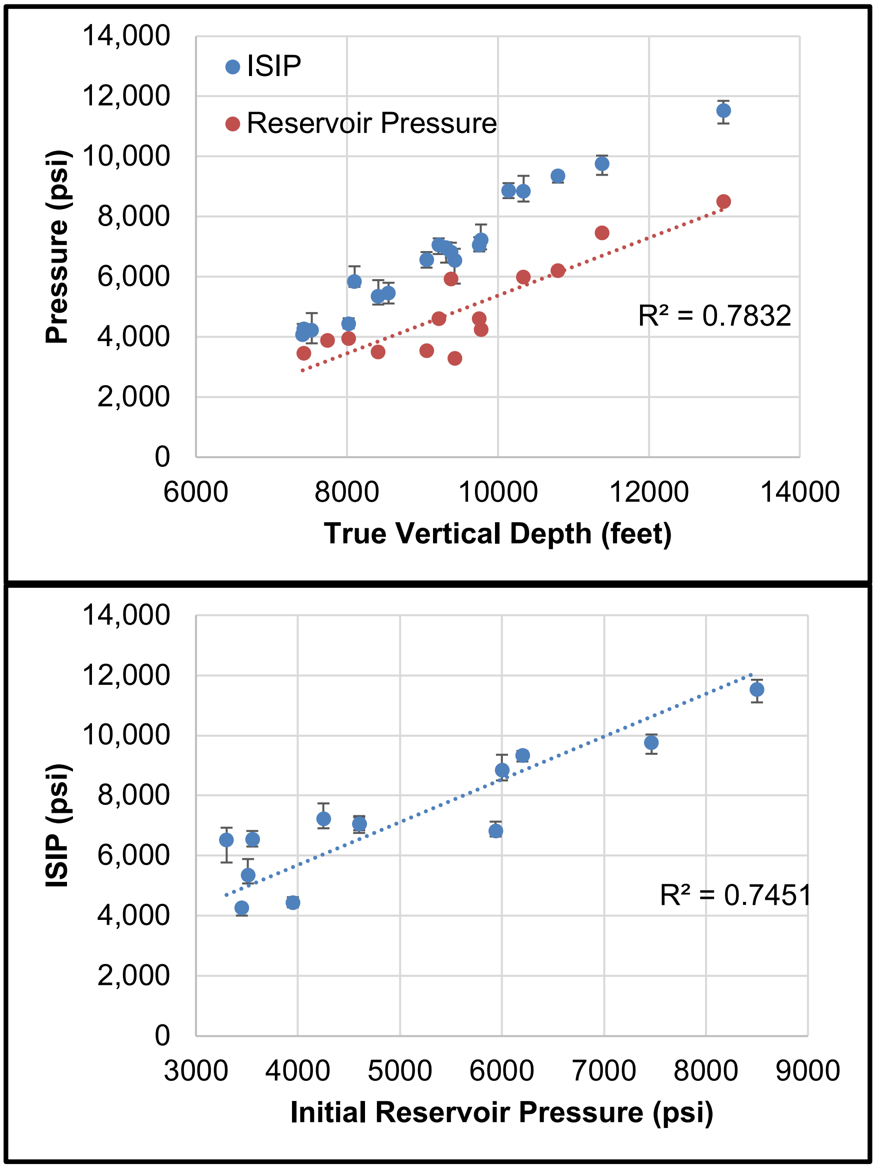

Figure 7–Comparison of interpreted initial reservoir pressure and average reported ISIP. Error bars represent the range from the 10th to 90th percentile of reported ISIP.

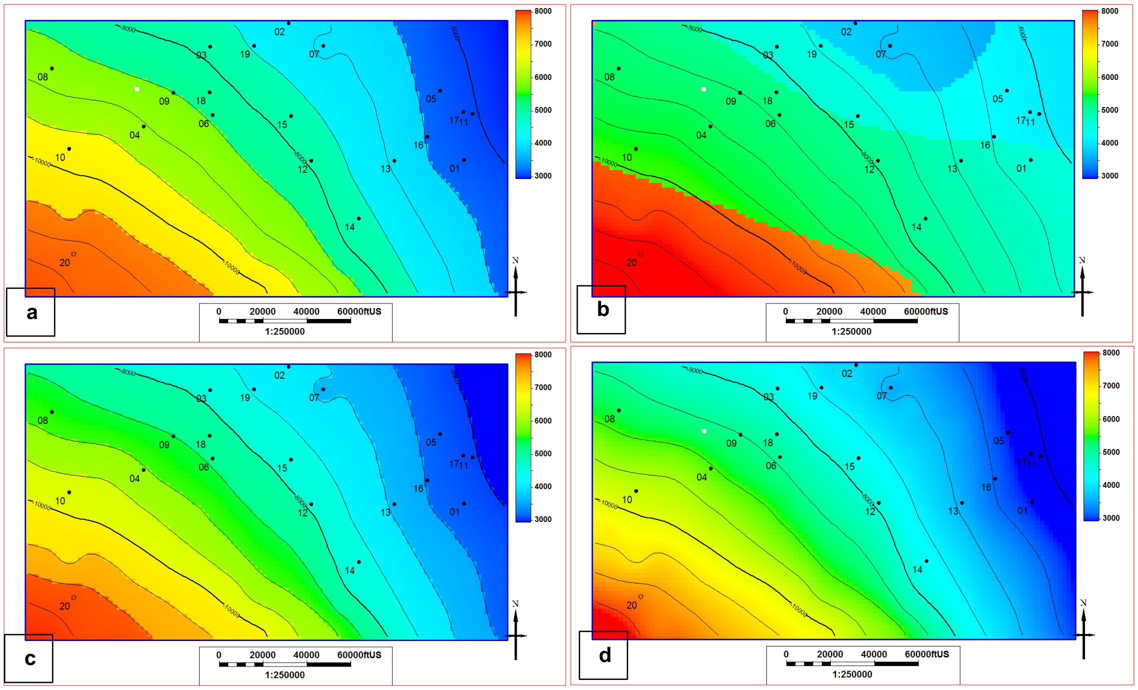

Figure 8–Initial reservoir pressures for Case 1-4, (a)-(d) respectively.

Arguably, the most valuable result of this workflow is a fluid characterization that can be applied to the entire region. As previously mentioned, the objective function used to tune the fluid model is based on the mismatch in initial producing gas-oil ratio. Compositional gradients were used as the primary tuning parameter. The resulting distribution of methane and the first plus fraction are shown in Figure 9 and are found to correspond well with the results presented by Welker et al. (2016). That study also found a relatively smooth increase in methane composition with depth and a decrease in heptane with depth within the study area. (As all four cases use the same compositional gradients, the distributions are practically identical; therefore, only the gradients from Case 1 are shown herein.)

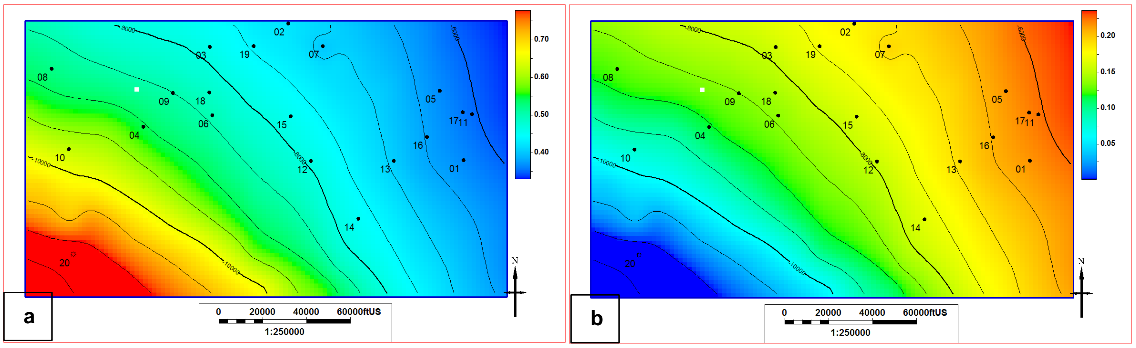

Figure 9–Fractional molar concentration distribution of (a) methane and (b) the first plus fraction.

As the objective of the EOS tuning was to match the initial producing GOR, it is critical to evaluate the quality of the match. Table 3 gives the results of the GOR match and is classified into three groups based on match quality. It should be noted that simulated GOR values do not vary much from case to case despite differences in initial pressure regimes. This similarity is due to two factors: compositional gradients are the same for each case and in all cases the reservoir is initially above saturation pressure. If the reservoir was initially below saturation pressure, different compositional gradients would need to be imposed on each case to achieve a match. The initial producing GOR for three wells, one of each match quality, is shown in Figure 10. Well-03, shown in Figure 10a, shows a good quality match and Well-16, shown in Figure 10b, shows a decent match. Well-02, shown in Figure 10c, shows a poor match. Well-02 was initially produced using a pump, not free flowing, and this could contribute to producing GOR behavior being different than what the model predicts.

Well	Observed GOR, MSCF/STB	Baffle Case 1 Simulated GOR, MSCF/STB	Baffle Case 2 Simulated GOR, MSCF/STB	Baffle Case 3 Simulated GOR, MSCF/STB
01	1.1	0.9	1.0	1.0
02	0.6	1.3	1.3	1.3
03	1.8	1.7	1.7	1.7
04	2.5	2.8	2.8	2.8
05	1.3	0.9	0.9	0.9
06	2.8	2.1	2.1	2.1
07	1.1	1.2	1.2	1.4
08	2.7	2.3	2.3	2.3
09	1.9	2.2	2.2	2.2
10	6.1	4.3	4.3	4.3
11	1.4	0.9	0.9	0.9
12	2.1	1.7	1.7	1.7
13	1.2	1.2	1.2	1.2
14	2.0	1.7	1.7	1.6
15	1.1	1.6	1.6	1.6
16	0.9	1.0	1.0	1.0
17	0.9	0.9	0.9	0.9
18	2.6	2.0	2.0	2.0
19	3.3	1.5	1.5	1.5
20	1,300	1,400	1,400	1,400

Table 3–Tabulation of the initial producing GOR history match quality. Colored according to error as follows: green: within 10%; yellow: within 50%; red: greater than 50%

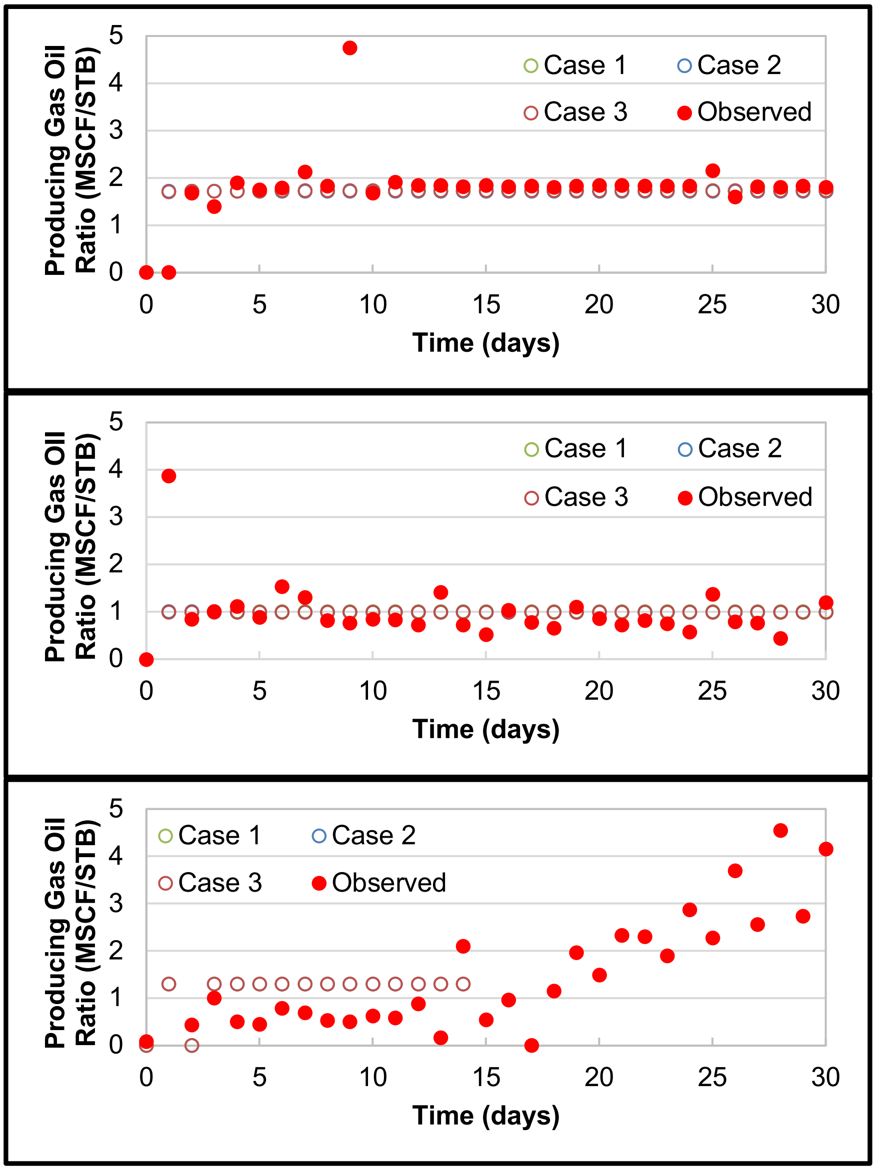

Figure 10–Comparison of observed and simulated GOR for Well 03 (a), Well 16 (b), and Well 02 (c).

To further test the validity of the fluid model, I qualitatively look at the evolution of GOR with respect to the bottomhole flowing pressure. Figure 11 shows p_{wf} and GOR relationships with time for two wells. The plots also indicate the predicted saturation pressure from the fluid model. In both cases, GOR remains relatively steady until BHP declines below the predicted saturation pressure, as would be expected, giving further credibility to the fluid model.

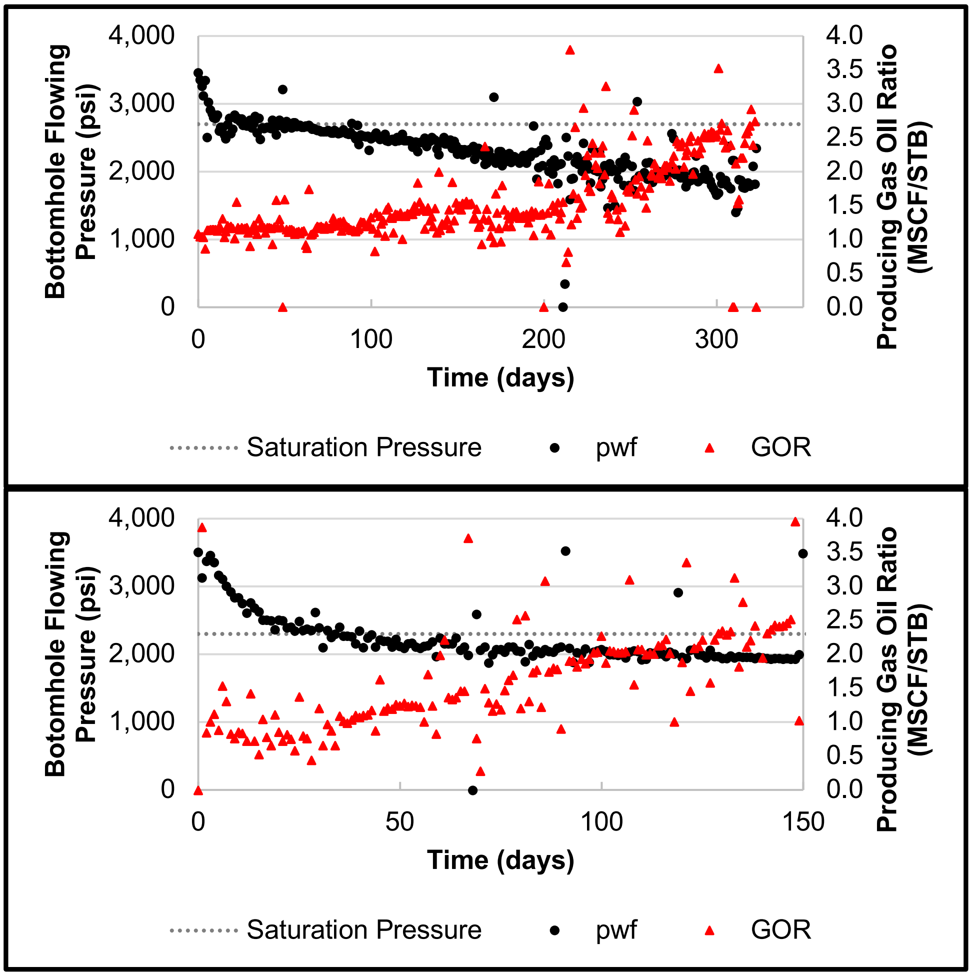

Figure 11–Bottomhole flowing pressure and producing GOR for Well 15 (a) and Well 07 (b). The period of constant GOR ends around the time the BHP declines below the predicted bubblepoint.

Thus far, I have sought to provide some validation of the fluid model. Only once the model can be proven to be a plausible representation of the reservoir should it be extrapolated across the region. Now that this has been done, we can extract important fluid properties and their distribution throughout the region: initial solution gas-oil ratio (R_{si}), initial vapor oil-gas ratio (R_{vi}), oil formation volume factor (B_o), gas formation volume factor (B_g), oil viscosity (μ_o), and saturation pressure (p_{sat}). For sake of conciseness, I only present R_{si} and B_o for all cases, in Figure 13 & 15 respectively, while Figure 12 & 14 presents R_{vi} and B_g alongside their respective oil properties.

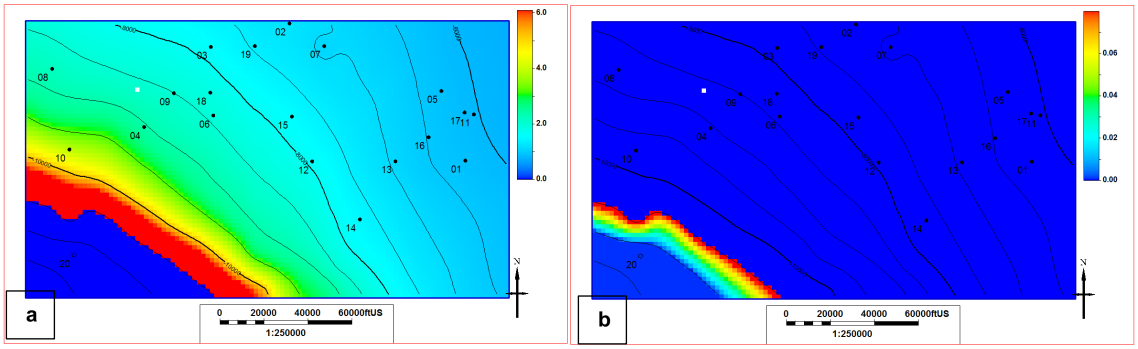

Figure 12–Solution gas-oil ratio (a) and vapor oil-gas ratio (b) for case 1.

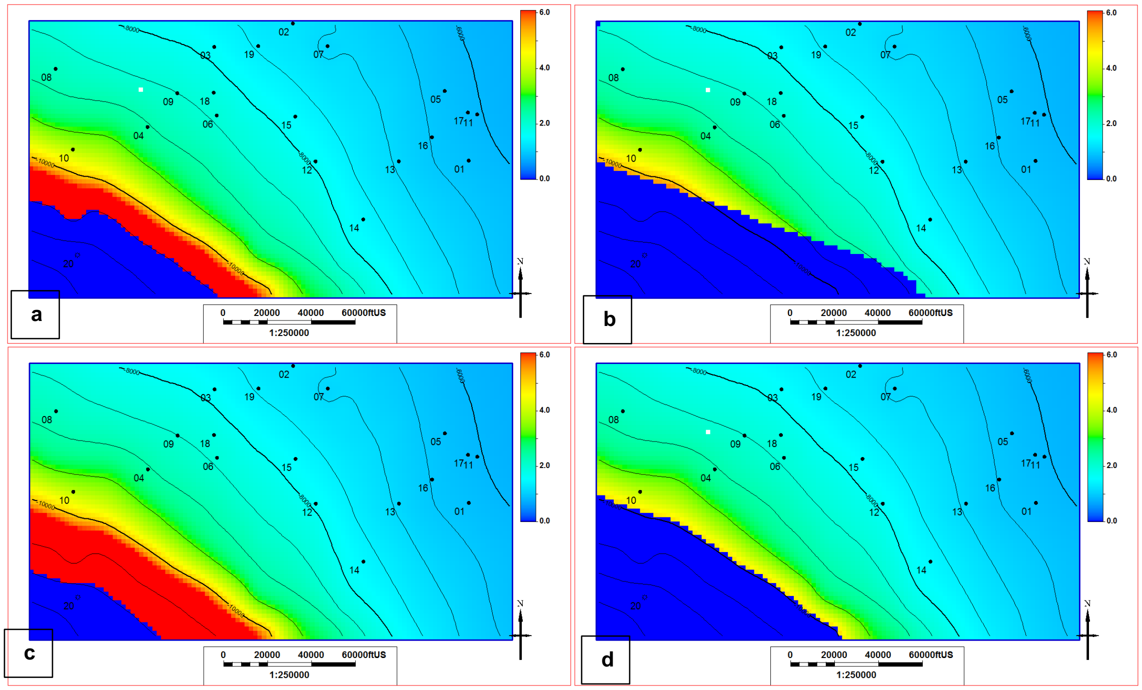

Figure 13–R_{si} for cases 1-4, (a)-(d) respectively.

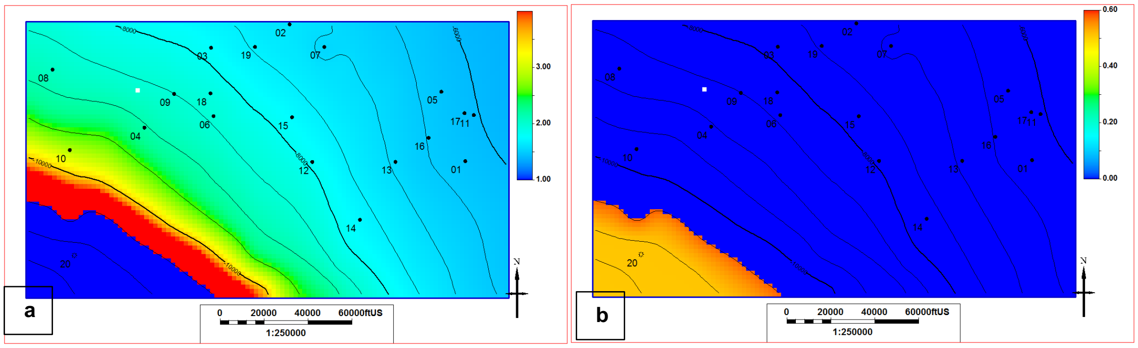

Figure 14–Oil formation volume factor (a) and gas formation volume factor (b) for case 1.

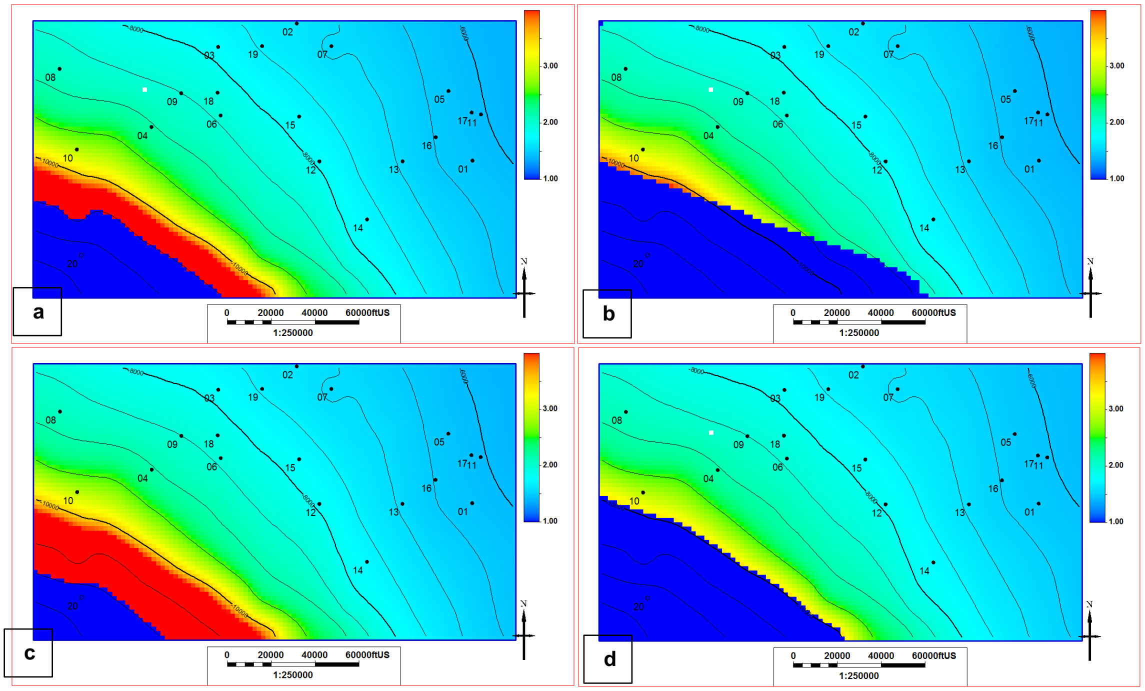

Figure 15–Oil formation volume factors for cases 1-4, (a)-(d) respectively.

In addition to the regional fluid characterization, the workflow yields information about the petrophysics and completions of the wells through RTA. Of the twenty wells in the study, six had quality enough pressure data to perform RTA. The analysis was completed with commercial software by using regression to match rate-time and pressure-time plots, as well as matching the log-log and Blasingame plots common to RTA (Palacio 1993 & Agarwal 1998). Sample log-log and Blasingame plots for Well-07 are given in Figure 16.

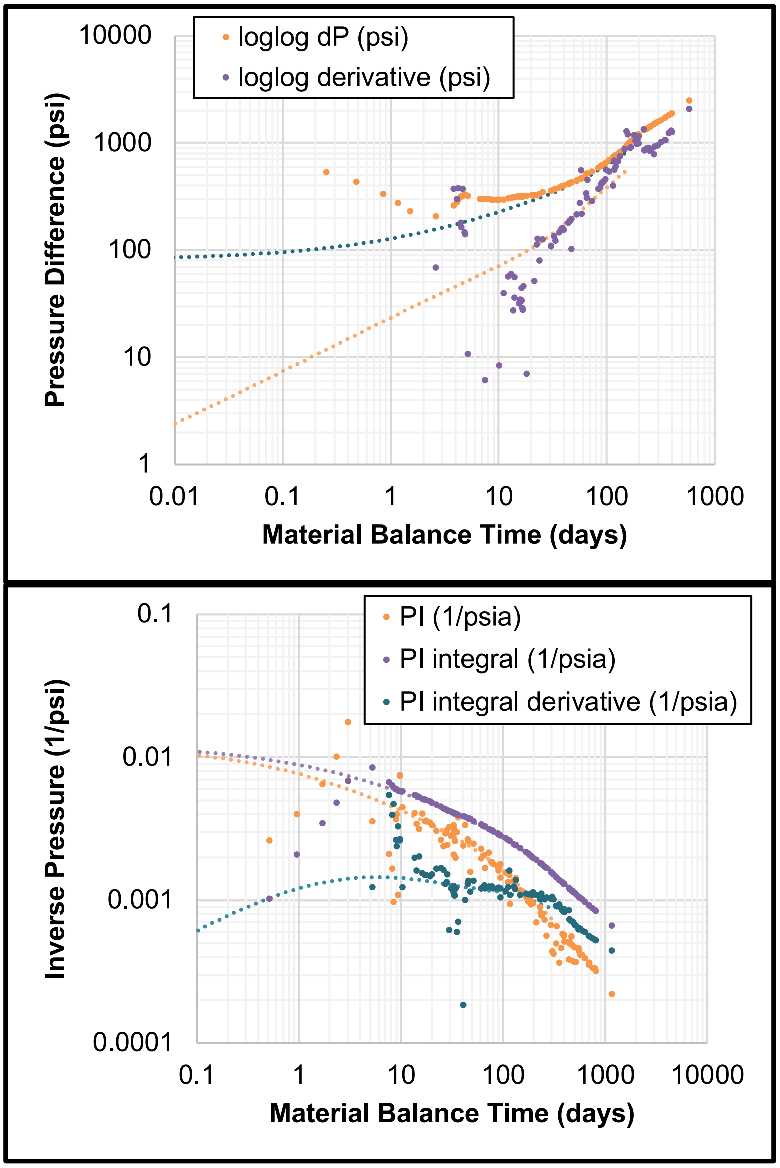

Figure 16 – Sample log-log and Blasingame plots as used in RTA, taken from Well 07.

The relevant results from RTA are shown in Table 4. (Skin values are not reported as they were all found to be at or near zero.) As mentioned in the methodology section, there were many unknown parameters that were used as regression variables when doing the RTA. Through pursuing four hypotheses and using two different reservoir models in RTA, we are afforded a range of values for each of those unknown parameters which allows for an estimation of the uncertainty in the results, as shown in

Table 4. It should be noted that although some values show no uncertainty, this should not be taken as a claim that the value is inherently correct; zero standard deviation simply means that the different models did not result in a different value for that variable.

	Well 01	Well 03	Well 07	Well 10	Well 15	Well 16
Permeability, μd	3 ± 2	2 ± 0.5	3 ± 0.5	30 ± 7	3 ± 2	1 ± 0.5
Thickness, ft	300 ± 0	200 ± 0	230 ± 1	207 ± 2	300 ± 0	275 ± 20
Porosity, %	8 ± 0.5	6 ± 1	8 ± 0.5	7 ± 0.5	8 ± 0	8 ± 0.5
Drainage Area, acres	380 ± 50	390 ± 150	390 ± 70	315 ± 110	505 ± 95	350 ± 45
Fractures	22 ± 3	23 ± 1	40 ± 15	20 ± 10	25 ± 5	27 ± 2
Fracture half length, ft	690 ± 80	730 ± 40	740 ± 100	540 ± 250	900 ± 160	640 ± 110
Fracture height, ft	300 ± 0	200 ± 0	232 ± 4	203 ± 3	300 ± 0	267 ± 26
Log(Fracture Conductivity), log(md·ft)	5 ± 1	7 ± 0	6 ± 2	8 ± 1	8 ± 1	9 ± 1

Table 4–Tabulation of RTA output parameters. Average value and standard deviation for all cases are reported.

Chapter 4: Single Well Hydraulic Fracture Modeling

This chapter will discuss the efforts to history match models to the hydraulic fracturing process for a single well: Well 07 from the Meramec data set. The ultimate goal of this work was to gain an understanding of the size of the resulting stimulated reservoir volume (SRV). Ultimately this work leads into Chapter 6, where I discuss efforts to forecast recovery from this well and Meramec generally. Within this chapter, I will first cover the history matching process as implemented using a flow simulator. After that I will cover the use of a fracture simulator and compare the results of both methodologies.

4.1 Completion History Matching with Flow Simulator

In this section I will discuss history matching of hydraulic fracturing injection with the use of a flow simulator. In short, beginning with a dual porosity model with highly conductive fractures, I history match the injection of fracturing fluid. Once this match is achieved, the results are used to interpret the size and extent of the stimulated reservoir volume. From here, the fracture properties are adjusted such that only the stimulated volume fractures are conductive, and the history is matched again with this adjusted model. The final model is a dual porosity model, where the fracture component is intended to represent the induced network from hydraulic fracturing.

4.1.1 Static Model Preparation

Using the full reservoir model framework introduced in Chapter 3, and an abundance of offset wells in the area, total porosity logs were created using the root-mean square calculation from density porosity and neutron porosity logs. These calculated logs were then used to generate a total porosity model for the entire study area with the use of Sequential Gaussian Simulation; inputs for variogram parameters were a 5,000 ft lateral range and 5 ft vertical range. From this region-wide reservoir model, a 6,000 ft by 13,000 ft model was extracted and refined around Well 07 to be used to model the hydraulic fracturing process. The resulting model has cell size of 100’x100’x3’ with 2,090,400 total grid cells. The zones of this smaller model are shown in Figure 17, and the total porosity model is shown in Figure 18. Available core data in the area allowed for generation of a permeability model by log-normal co-kriging with the given porosity model using inputs of mean and standard deviation. Resulting permeability model is shown in Figure 19.

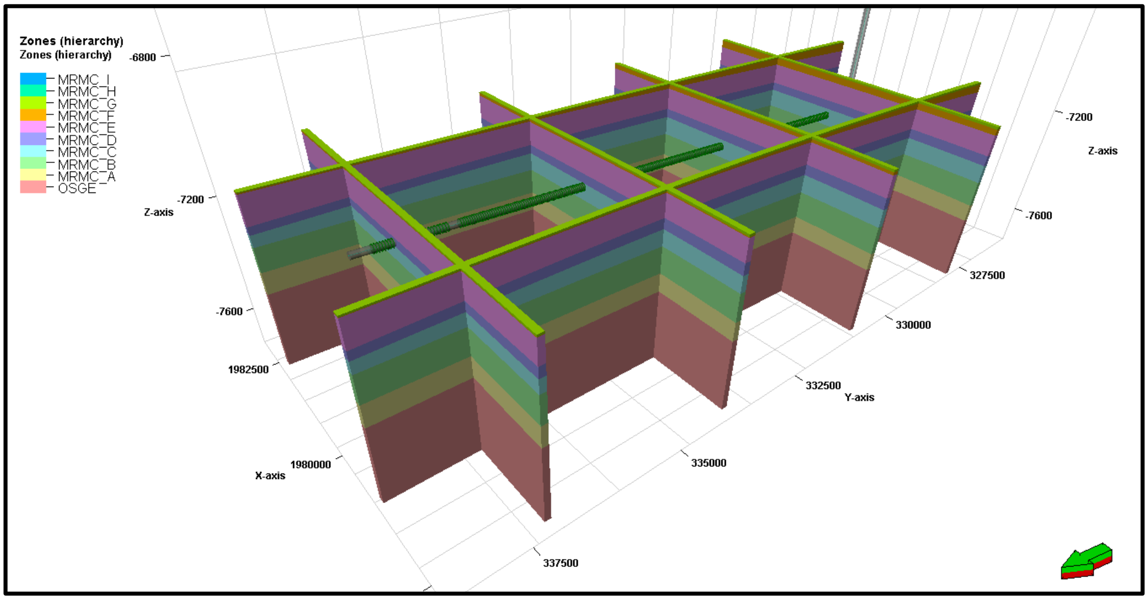

Figure 17–Zones of refined model around Well 07.

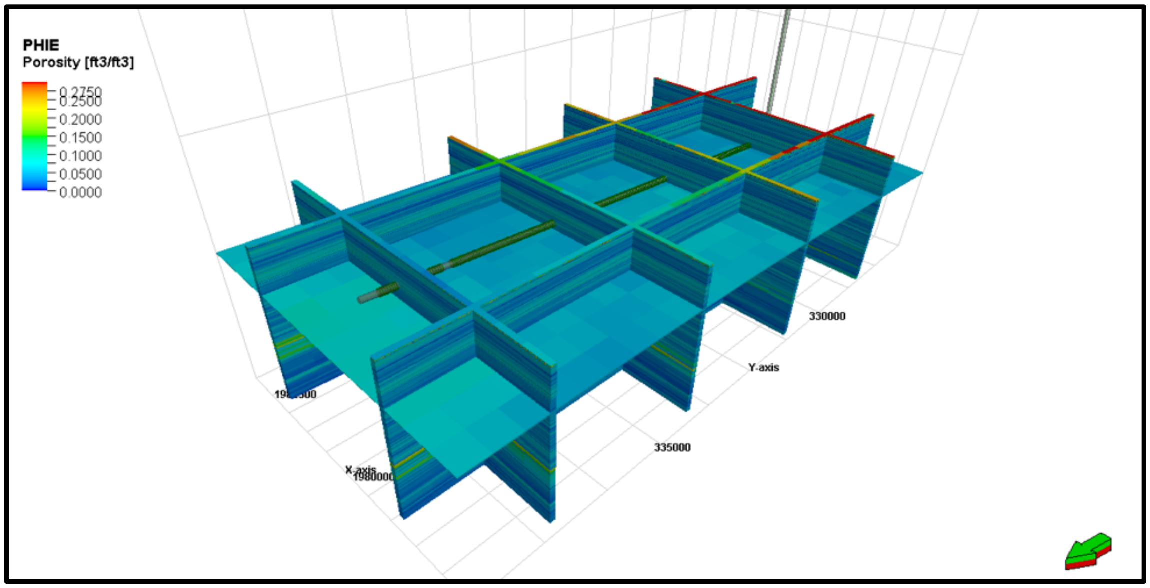

Figure 18–Total porosity model from petrophysical modeling. This model is used in the simulations that follow

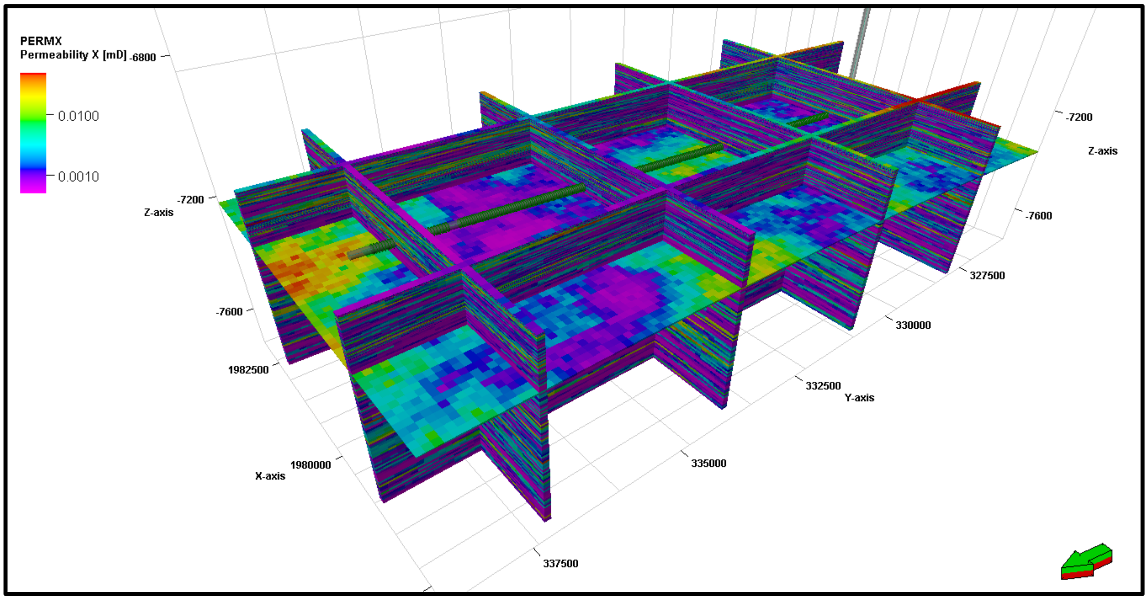

Figure 19–Permeability of refined model around Well 07.

Further, the compositional fluid model generated in Chapter 3 was used to generate a black oil fluid model with similar properties to be used in this phase of the project. A black oil model was used to decrease computational time. The black oil model was generated by initializing two different reservoir models, one with the compositional fluid model and one with the black oil model, and then tuning the inputs of the black oil model such that oil formation volume factors, fluid densities, solution gas-oil ratios, and initial reservoir pressures of the two models agree.

4.1.2 Well Design and Injection History

Perforations are added to the well according to the completion report. Stage by stage injection volumes and times were used as inputs for the well. This injection scheme is shown in Table 5.

Stage	Start Time, dd:hh:mm	End Time, dd:hh:mm	Duration, hr	Fluid Total, gal
1	00:10:00	00:11:30	1.50	172,410
2	01:00:00	01:02:00	2.00	179,886
3	07:15:45	07:22:00	6.25	632,898
4	08:02:30	08:05:30	3.00	232,134
5	08:09:00	08:11:15	2.25	217,671
6	08:14:45	08:17:00	2.25	216,821
7	08:20:15	08:22:45	2.50	225,246
8	09:04:30	09:07:00	2.50	216,468
9	09:08:30	09:10:45	2.25	199,385
10	09:16:15	09:19:00	2.75	198,666
11	09:20:15	09:23:00	2.75	229,961
12	10:03:45	10:06:15	2.50	227,272
13	10:10:30	10:13:15	2.75	219,087
14	10:16:45	10:19:00	2.25	224,349
15	10:22:00	11:00:30	2.50	225,440
16	11:05:45	11:08:00	2.25	224,349
17	11:09:45	11:13:00	3.25	214,425
18	11:17:30	11:19:45	2.25	218,427
19	11:22:30	12:00:45	2.25	217,712
20	12:03:45	12:06:15	2.50	219,435
21	12:14:00	12:16:30	2.50	206,877
22	12:18:45	12:21:00	2.25	215,402
23	13:00:00	13:02:15	2.25	224,181
24	13:04:30	13:06:45	2.25	208,989
25	13:10:30	13:12:45	2.25	215,602
26	13:15:00	13:17:30	2.50	210,321
27	13:19:30	13:21:45	2.25	207,338
28	14:00:30	14:02:30	2.00	204,189
29	14:04:45	14:07:00	2.25	203,391
30	14:10:00	14:12:00	2.00	202,245
31	14:13:45	14:16:00	2.25	198,046
32	14:18:00	14:20:15	2.25	195,996
33	14:22:15	15:00:30	2.25	196,970
34	15:03:15	15:05:30	2.25	197,716

Table 5–Injection history of completion of Well 07.

4.1.3 Rock Compaction

Permeability tests on 26 available cores show permeability values at two different confining pressures, 1000 and 2800 psia. This data is shown in Figure 20. From this data I was able to extract a range of possibilities for how permeability will likely be enhanced by the increase in pressure brought on through hydraulic fracturing. According to Bhandari et al. (2015), permeability varies with confining stress according to **Eq. 2**. For each core the two available data points were used to compute m and b from Eq. 2; a sample best fit line is shown in Figure 20. Resulting values for m from all samples are shown in the histogram in Figure 21. Initially, the median for m was used, but m will also be treated as a tuning parameter during history matching.

$$k = b * e^{m\sigma_{eff}} \qquad (2)$$

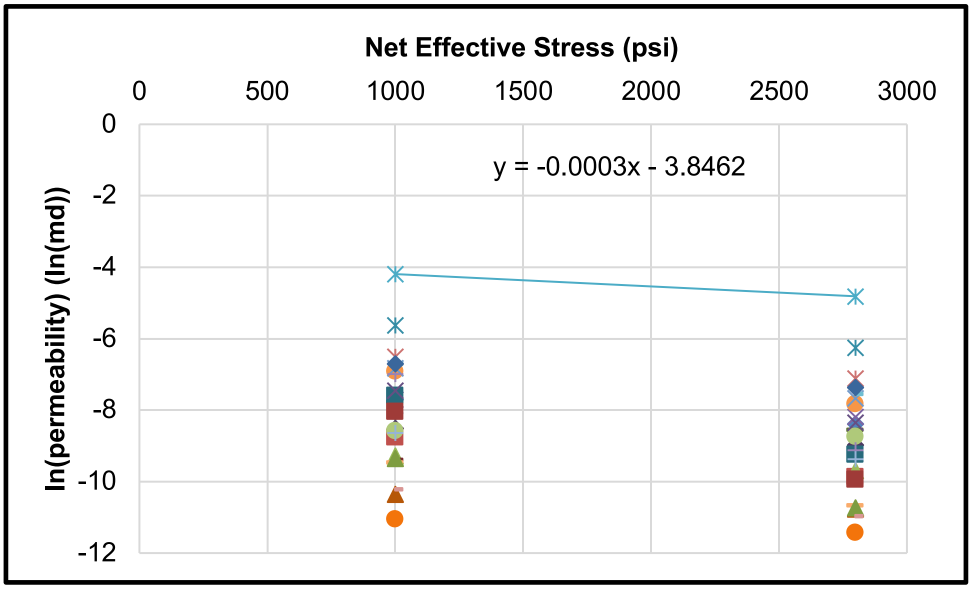

Figure 20–Core permeability values at two different net effective stresses. A sample best fit according to Eq. 2 is shown for one core.

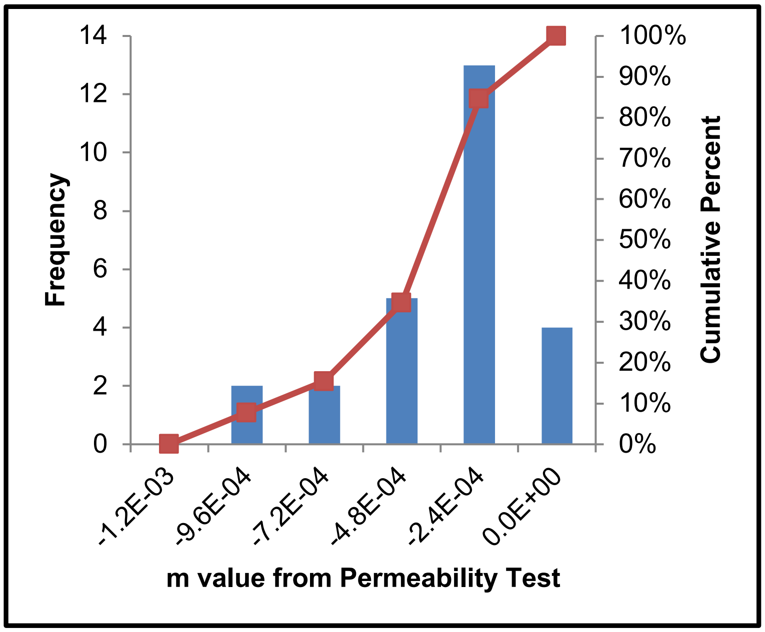

Figure 21–Histogram of calculated m values from core data.

From this data I am able to tabulate a rock compaction table. While the data in this table is later used to history match, the base case rock compaction is shown in Table 6. Due to the fact that the fractures will propagate in the x- and z-directions, the transmissibility multipliers are applied mainly in these directions.

Net Stress	Multipliers			
	Porosity	x-Transmissibility	y-Transmissibility	z-Transmissibility
9000	0.94	0.06	0.96	0.06
4000	0.95	0.44	0.97	0.44
2000	0.99	1	0.99	1
0	1.01	2.29	1	2.29
-2000	1.07	5.23	1	5.23

Table 6–Tabulation of base case rock compaction parameters.

4.1.4 Dual Porosity Setup

For the next step in model generation, a natural fracture network was generated. Initially, the fractures were assigned properties (permeability and matrix-fracture interaction) similar to those expected from an induced hydraulically fractured network. Later in the history matching process, the fracture properties will be modified such that only the area around the wellbore is enhanced to have these high values. However, by starting with these enhanced values throughout the model instead of imposing an enhanced region from the beginning of history matching, I am hoping to remain unbiased toward any particular size or shape of stimulated reservoir volume (SRV).

4.1.5 Initial Match with Large Fracture Network

After simulation case creation, design of experiments was used to highlight parameters that have the greatest effect on the quality of the match. Several parameters were treated as uncertain and are listed in Table 7 along with a description of the parameter. A Plackett-Burman design was used to generate cases, with the base, minimum, and maximum parameter values shown in Table 8.

Identifier	Description
KZKX	Vertical to horizontal permeability ratio
KYKX	y- to x- directional permeability ratio
PERM	Matrix permeability modification factor
FRACPERMMULT	Fracture permeability modification factor
PORO	Matrix porosity modification factor
SIGMA	Matrix-fracture interaction modification factor
KRWSORW	Water relative permeability at residual oil saturation
SORW	Residual oil saturation
SWCR	Critical water saturation
WCOREY	Corey exponent for water
TMexpm	e raised to the slope exponent from Eq. 2
PM9	Porosity modifier at 9000 psi effective stress
PM4	Porosity modifier at 4000 psi effective stress
PM2	Porosity modifier at 2000 psi effective stress
PM0	Porosity modifier at 0 psi effective stress
PMN	Porosity modifier at -2000 psi effective stress
TMX9	x-direction transmissibility modifier at 9000 psi effective stress
TMX4	x-direction transmissibility modifier at 4000 psi effective stress
TMX2	x-direction transmissibility modifier at 2000 psi effective stress
TMX0	x-direction transmissibility modifier at 0 psi effective stress
TMXN	x-direction transmissibility modifier at -2000 psi effective stress
TMY9	y-direction transmissibility modifier at 9000 psi effective stress
TMY4	y-direction transmissibility modifier at 4000 psi effective stress
TMY2	y-direction transmissibility modifier at 2000 psi effective stress
TMY0	y-direction transmissibility modifier at 0 psi effective stress
TMYN	y-direction transmissibility modifier at -2000 psi effective stress
TMZ9	z-direction transmissibility modifier at 9000 psi effective stress
TMZ4	z-direction transmissibility modifier at 4000 psi effective stress
TMZ2	z-direction transmissibility modifier at 2000 psi effective stress
TMZ0	z-direction transmissibility modifier at 0 psi effective stress
TMZN	z-direction transmissibility modifier at -2000 psi effective stress

Table 7–Definitions of parameters used in first experiment.

Parameter	Base Value	Minimum Value	Maximum Value
KZKX	0.05	0.005	0.1
KYKX	1	0.5	2
PERM	1	1	10
FRACPERMMULT	10000	10000	50000
PORO	1	0.8	1.2
SIGMA	1	0.75	1.3
KRWSORW	0.7	0.6	0.8
SORW	0.14	0.1	0.18
SWCR	0.3	0.2	0.35
WCOREY	4	3	4.5
TMexpm	0.999586	0.999414	0.999662
PM9	0.94	0.9	0.95
PM4	0.99	0.95	0.995
PM2	1	0.995	1.02
PM0	1.04	1.02	1.05
PMN	1.07	1.05	1.1
TMX9	0.06	TMexpm^(9000-2000)	
TMX4	0.44	TMexpm^(4000-2000)	
TMX2	1	1	1
TMX0	2.29	TMexpm^(0-2000)	
TMXN	5.23	TMexpm^(-2000-2000)	
TMY9	0.96	0.94	0.965
TMY4	0.97	0.965	0.98
TMY2	0.99	0.98	1
TMY0	1	1	1
TMYN	1	1	1.05
TMZ9	0.06	TMexpm^(9000-2000)	
TMZ4	0.44	TMexpm^(4000-2000)	
TMZ2	1	1	1
TMZ0	2.29	TMexpm^(0-2000)	
TMZN	5.23	TMexpm^(-2000-2000)	

Table 8–Case parameters for first experiment.

After the cases from the first experiment were run, the impact of each parameter on match quality (relative to cumulative water injection) was analyzed with a Pareto plot (Figure 22). As is readily observed, the most impactful parameters, unsurprisingly, were the fracture permeability multiplier and the vertical to horizontal permeability ratio. The upper and lower bounds are adjusted accordingly for a second experiment, with parameters shown in Table 9. In addition to these two parameters being adjusted, a new parameter, 'KZKXFRAC', is introduced representing the vertical to horizontal fracture permeability ratio.

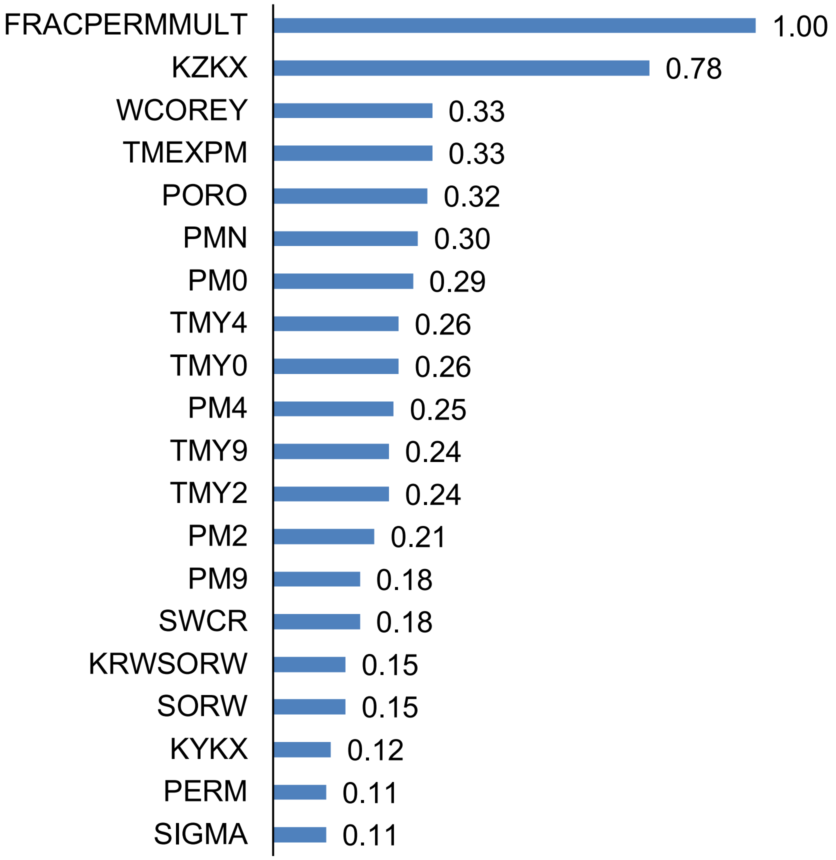

Figure 22–Pareto plot from results of first experiment.

Parameter	Base Value	Minimum Value	Maximum Value
KZKX	0.05	0.01	0.1
KYKX	1	0.5	2
PERM	1	1	10
FRACPERMMULT	50000	25000	75000
PORO	1	0.8	1.2
SIGMA	1	0.75	1.3
KRWSORW	0.7	0.6	0.8
SORW	0.14	0.1	0.18
SWCR	0.3	0.2	0.35
WCOREY	4	3	4.5
TMexpm	0.999586	0.999414	0.999586
PM9	0.94	0.9	0.95
PM4	0.99	0.95	0.995
PM2	1	0.995	1.02
PM0	1.04	1.02	1.05
PMN	1.07	1.05	1.1
TMX9	0.06	TMexpm^(9000-2000)	
TMX4	0.44	TMexpm^(4000-2000)	
TMX2	1	1	1
TMX0	2.29	TMexpm^(0-2000)	
TMXN	5.23	TMexpm^(-2000-2000)	
TMY9	0.96	0.94	0.965
TMY4	0.97	0.965	0.98
TMY2	0.99	0.98	1
TMY0	1	1	1
TMYN	1	1	1.05
TMZ9	0.06	TMexpm^(9000-2000)	
TMZ4	0.44	TMexpm^(4000-2000)	
TMZ2	1	1	1
TMZ0	2.29	TMexpm^(0-2000)	
TMZN	5.23	TMexpm^(-2000-2000)	
KZKXFRAC	0.1	0.05	0.2

Table 9–Case parameters for second experiment.

From the results of this experiment, actually one generated test model was found to have a satisfactory match, so it was carried forward into the next phase of the process.

4.1.6 Refined Match with Enhanced Region

After attaining a match with one model, the pressure distribution after fracturing is used to highlight the region around the wellbore that will be a part of the stimulated reservoir volume (SRV). Through application of a filter that shows which cells have a net effective stress that has been raised above base value, the resulting SRV can be visualized, as shown in Figure 23. The half-length of this resulting volume is 550 ft and the resulting height is 260 ft.

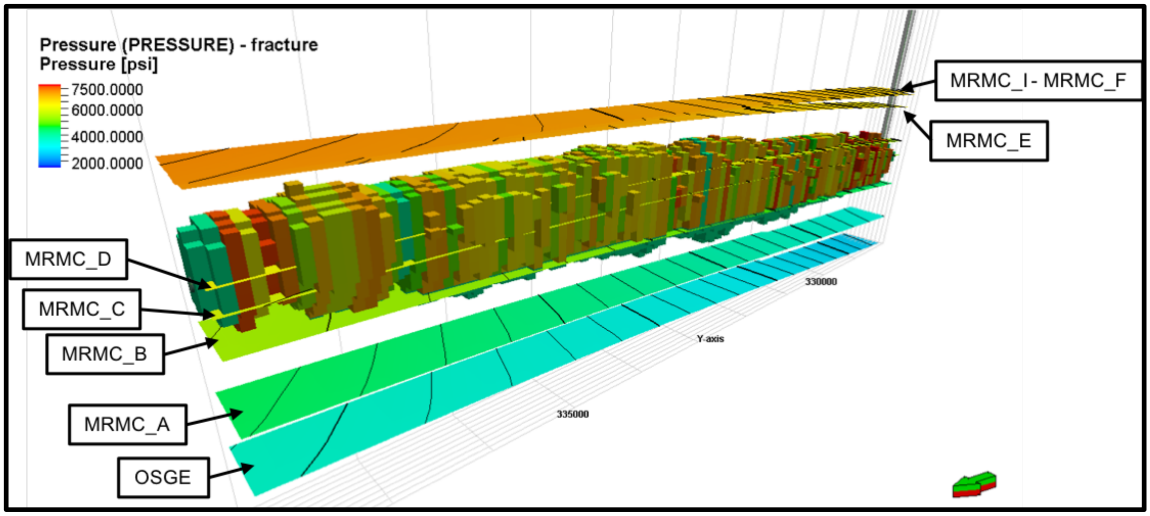

Figure 23–Visualization of SRV from stress filter, shown at 7.5x vertical exaggeration.

From here, the natural fracture parameters are set to background matrix values, and only within the enhanced region are the fracture permeability and matrix fracture interaction raised to levels expected from an induced, hydraulically fractured network. From the increase in net effective stress, transmissibility multipliers for both the fractures and matrix are calculated; **Eq. 3** shows this calculation. This new model is then history matched to water injection volumes from the completion report, using the exponent ‘a’ as the primary history matching parameter. Relative to the fractures, it is assumed that the transmissibility modification occurs primarily in the x- and z-directions. The resulting history match is shown in Figure 24. Resulting values of ‘a’ are 16 for the x- and z- directions, and 4 for the y-direction.

$$TM = \left(\frac{\sigma_{net\_init}}{\sigma_{net\_min}}\right)^{a} \quad , \ldots\ldots\ldots\ldots\ldots\ldots\ldots\ldots\ldots\ldots\ldots\ldots\ldots\ldots \quad (3)$$

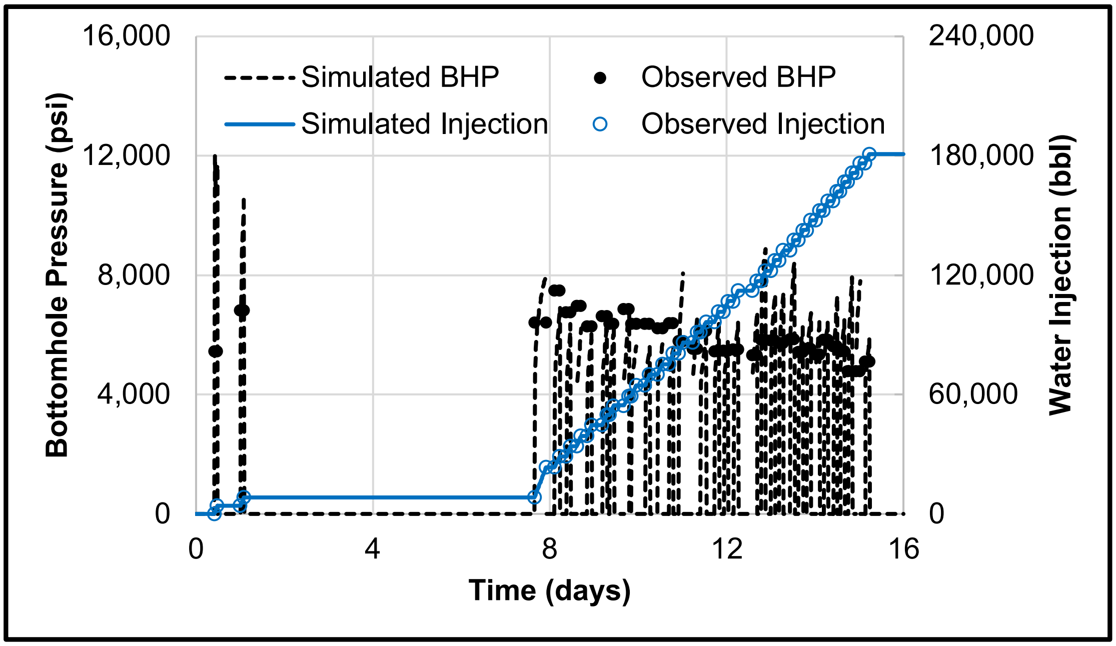

Figure 24–Observed and simulated values for completion of Well 07.

4.2 Comparison to Fracture Simulator

With the model discussed above, a model is created in the GOHFER fracture simulator. Using the injection volumes and times presented in Table 5, with the addition of proppant concentrations shown in Table 10, a pumping schedule for the first 13 stages of Well 07 was generated. Using this pumping schedule and the model as inputs, I ran the fracture simulator. From the results, fracture cells with less than 0.1 md*ft of conductivity are filtered out and the points shown in Figure 25, represent the extent of the SRV. Approximate fracture half-length and height are 350 and 300 feet respectively. In comparing the results of the two methodologies, use of the flow simulator (Figure 26) predicts longer half-lengths and shorter heights than the fracture simulator.

Stage	Duration, hr	Fluid Total, gal	Proppant Concentration, lbs/gal
1	1.50	172,410	0.44
2	2.00	179,886	1.12
3	6.25	632,898	2.14
4	3.00	232,134	1.88
5	2.25	217,671	2.02
6	2.25	216,821	2.03
7	2.50	225,246	1.71
8	2.50	216,468	1.77
9	2.25	199,385	1.92
10	2.75	198,666	1.93
11	2.75	229,961	2.09
12	2.50	227,272	2.02
13	2.75	219,087	2.10

Table 10–Pumping schedule used in fracture simulation.

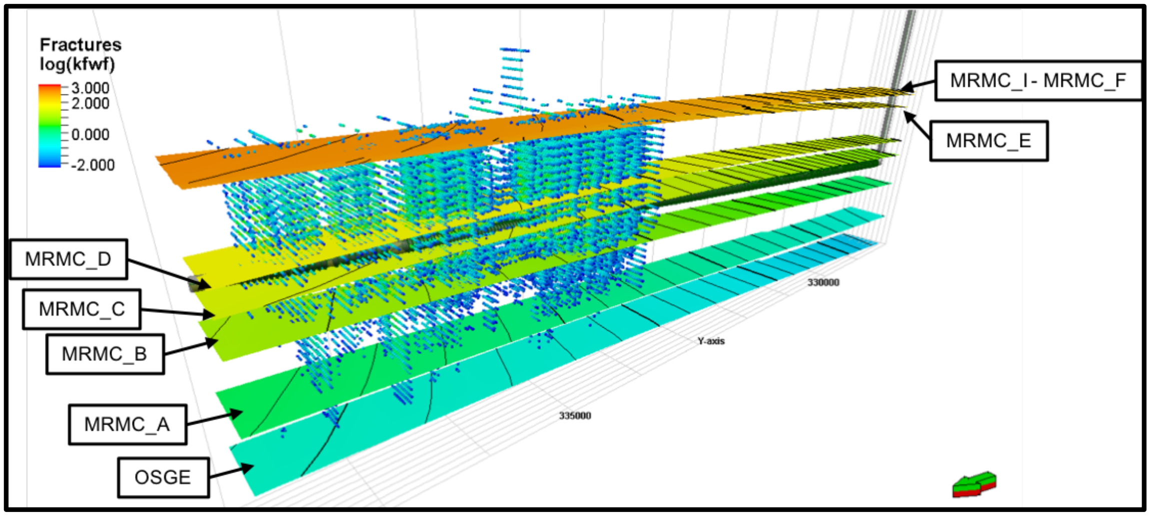

Figure 25–Depiction of resulting fractures from fracture simulator shown at 7.5x vertical exaggeration. Color corresponds to the log of fracture conductivity.

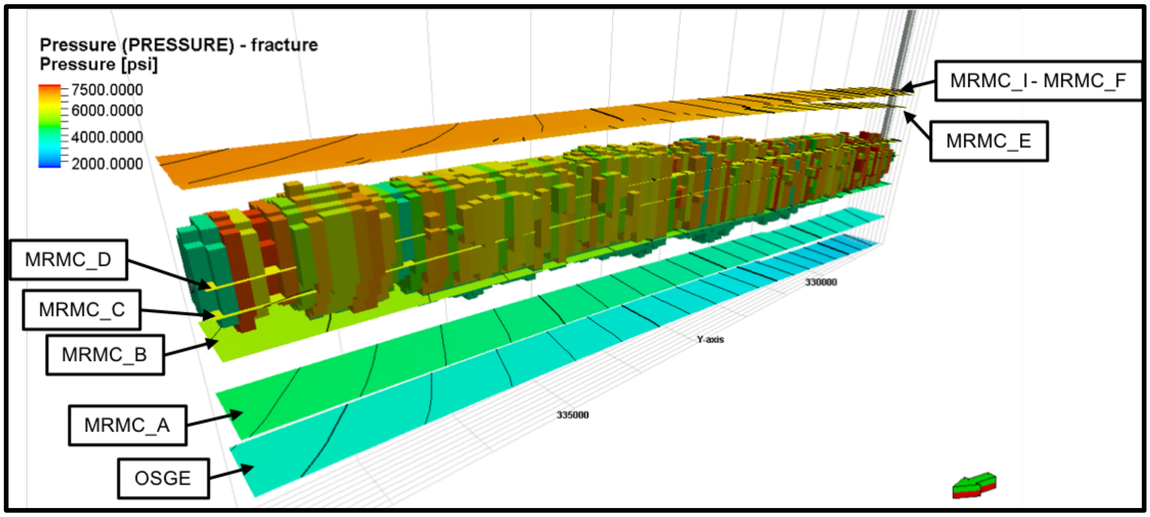

Figure 26–Restatement of SRV from flow simulator as shown in Figure 23.

The results from this work seem to lend to the idea that this methodology of using a flow simulator to generate the SRV is effective; the results are pretty similar between the flow simulator and the fracture simulator. Further, because the modeling work is already completed at this point, it makes for an easy transition from modeling of fracturing to the modeling of production.

Chapter 5: Fracture Diagnostics Using Modified Hall Method

This chapter will present a new methodology for diagnosing hydraulic fracture efficiency. It is an adapted methodology related to modified Hall Analysis, which allows for the detection of changes in injection well injectivity. I apply this concept to the injection of hydraulic fracturing fluid to understand if the method can be applied in this new manner.

5.1 Background and Hypothesis

Traditional Hall Analysis is used to identify plugging and fracturing behavior in injection wells. Here I adapt the traditional analysis techniques so the methodology can be applied to the hydraulic fracturing process and evaluate the efficacy of the adapted methods. Traditionally, the Hall Integral (HI) is computed according to **Eq. 4**, and the derivative of the Hall Integral is computed according to **Eq. 5**.

$$HI = \int_0^t \left(p_{wf} - p_e\right) dt \, , \qquad (4)$$

$$dHI = \frac{\Delta HI}{\Delta W_i} \, , \qquad (5)$$

Once both have been computed, plotting them against cumulative water injection (W_i) yields a diagnostic plot that allows for interpretation of the onset of fracturing and plugging. Example interpretations of this plot are shown in Figure 27; an increasing HI (increased dHI) indicates positive skin and a decreasing HI (decreased dHI) indicates negative skin (i.e. fracturing). To further outline this concept, what is being measured by the Hall Integral is the degree of pressure buildup. By comparing the HI with water injection, we can detect changes in injectivity. For example, if a decrease in the bottomhole pressure from one time to another corresponds with an appropriate decrease in water injection rate, we can say normal injection has continued, and the dHI should remain relatively unchanged. However, if a decrease in the bottomhole pressure corresponds with a steady or increasing injection rate, resulting in a decreasing dHI, we can interpret that something has occurred that has led to an increase in injectivity (i.e. fracturing). The goal of hydraulic fracturing is to increase injectivity (and corresponding productivity), so here I evaluate the applicability of the dHI concept in the evaluation of fracturing efficiency.

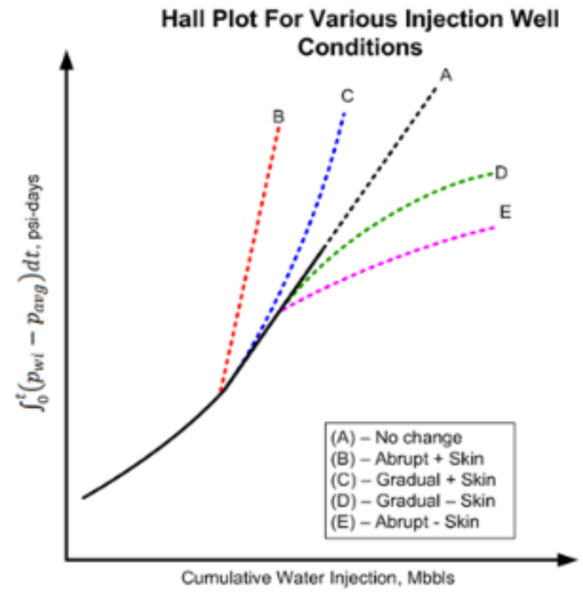

Figure 27–Illustration of Hall plot interpretation (Fekete, 2018).

The adapted methodology modifies the formulation for the HI to include the Initial Shut-In Pressure (ISIP) in place of the reservoir pressure at the boundary (p_e). The new formulations for HI and dHI are presented in **Eqs. 6-7**.

$$HI = \int_0^t (p_{wf} - ISIP)dt \; , \ldots\ldots (6)$$

$$dHI = \frac{\Delta HI}{\Delta W_i} \; , \ldots\ldots (7)$$

We hypothesize that with this new formulation, one should be able to use different aspects of the Hall plot to understand fracturing efficiency. We would expect to see increasing efficiency when dHI is decreasing relative to W_i and decreasing efficiency when dHI is increasing relative to W_i. If the hypothesis were to hold, this methodology would have three broad implications. First, it could be used on-site during fracture treatment to quickly diagnose which stages are creating better fractures and which have low efficiency. These learnings could be used in real-time to adjust treatment design. Second, it could be used to go back and evaluate old completions and provide diagnostics for fracture quality of the wells. This could have implications in future completion design and selection of cluster location along a lateral. Third, it can be used to compare completions in different wells. This type of comparison provides value in identifying well performance drivers as well as facilitating reservoir-wide completion-quality mapping.

5.2 Testing Methodology

In order to test this methodology, I ran 41 GOHFER fracture simulations with various job designs in order generate data that could be used to test the hypothesis. The designs were formulated using a Plackett-Burman experimental design. The designs are all used on a sample model provided by GOHFER. The designs all follow the same general structure and are implemented on a section of wellbore encompassing twenty perforation clusters. Each stage has an initial phase where the treating fluid carries proppant, a second phase where a flushing fluid is pumped with no proppant, and a final phase where the well rests, meant to simulate time where the previous stage is being plugged off and the new stage is being perforated. A typical pump schedule is shown in Figure 28. Within this generic framework, several parameters were varied in the experimental design. These parameters have been listed in Table 11.

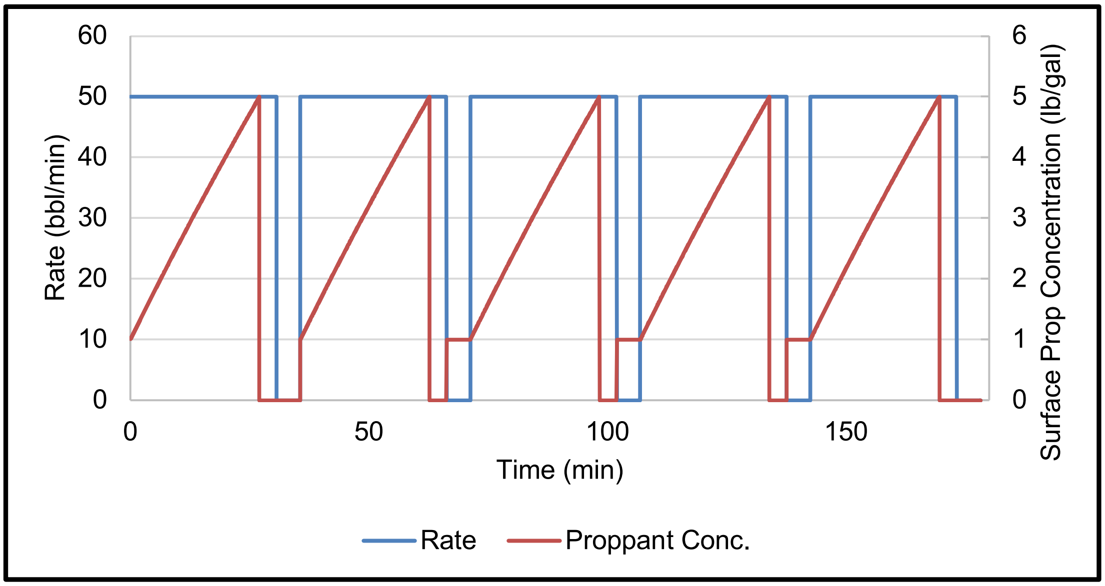

Figure 28–Typical pump schedule with phases of stage highlighted: green-treatment, blue-flush, and red-downtime.

Parameter	Min	Max
Cluster Spacing	50	75
Clusters per Stage	4	5
Total Clusters	20	20
Base Liquid Rate	50	70
Base Cumulative Liquid	50000	75000
Base Starting Proppant Concentration	2	3
Base Final Proppant Concentration	5	7
Variant Liquid Rate	60	90
Variant Cumulative Liquid	50000	65000
Variant Starting Proppant Concentration	3	5
Variant Final Proppant Concentration	6	8
Base Flush Rate	50	60
Base Flush Cumulative Liquid	7500	9000
Variant Flush Rate	60	50
Variant Flush Cumulative Liquid	7500	8500
Downtime	5	15
Base Cluster Efficiency	1	1
Variant Cluster Efficiency	0.50	0.75
Stages using Base Liquid Rate	1 3 5	1 2 3 4 5 6
Stages using Base Cumulative Liquid	1 3 5	1 2 3 4 5 6
Stages using Base Starting Proppant Concentration	1 3 5	1 2 3 4 5 6
Stages using Base Final Proppant Concentration	1 3 5	1 2 3 4 5 6
Stages using Variant Liquid Rate	2 4 6	0
Stages using Variant Cumulative Liquid	2 4 6	0
Stages using Variant Starting Proppant Concentration	2 4 6	0
Stages using Variant Final Proppant Concentration	2 4 6	0
Stages using Base Flush Rate	1 3 5	1 2 3 4 5 6
Stages using Base Flush Cumulative Liquid	1 3 5	1 2 3 4 5 6
Stages using Variant Flush Rate	2 4 6	0
Stages using Variant Flush Cumulative Liquid	2 4 6	0
Stages using Base Cluster Efficiency	1 3 5	1 2 3 4 5 6
Stages using Variant Cluster Efficiency	2 4 6	0

Table 11–Parameters used in Design of Experiments.

5.3 Verification of Hypothesis

For each of the cases, four parameters are calculated that can be treated as analogs for fracturing efficiency: total fracture area, total fracture volume, average fracture area, average fracture volume. These are calculated with **Eqs. 8-11**. Further, four features are extracted using the adapted dHI methodology presented in Section 5.1:

linear intercept, slope, and integral of dHI with respect to Wi, and the dHI computed from the averaged pressure and rate.

$$A_t = \sum h_{cell\_i} l_{cell\_i} \quad (8)$$

$$V_t = \sum h_{cell\_i} l_{cell\_i} w_{f\_i} \quad (9)$$

$$A_{ave} = \left(\sum h_{cell\_i} l_{cell\_i}\right)/n_f \quad (10)$$

$$V_{ave} = \left(\sum h_{cell\_i} l_{cell\_i} w_{f\_i}\right)/n_f \quad (11)$$

With four dependent variables, and four independent variables, there exist sixteen possible correlations between dHI behavior and fracturing efficiency. For each of these combinations, a correlation coefficient was computed for each of the 41 cases. The values of these correlation coefficients were tabulated to understand what, if anything, can be predicted from the adapted dHI methods. Histograms of correlation coefficients for each parameter set are shown in Figure 29.

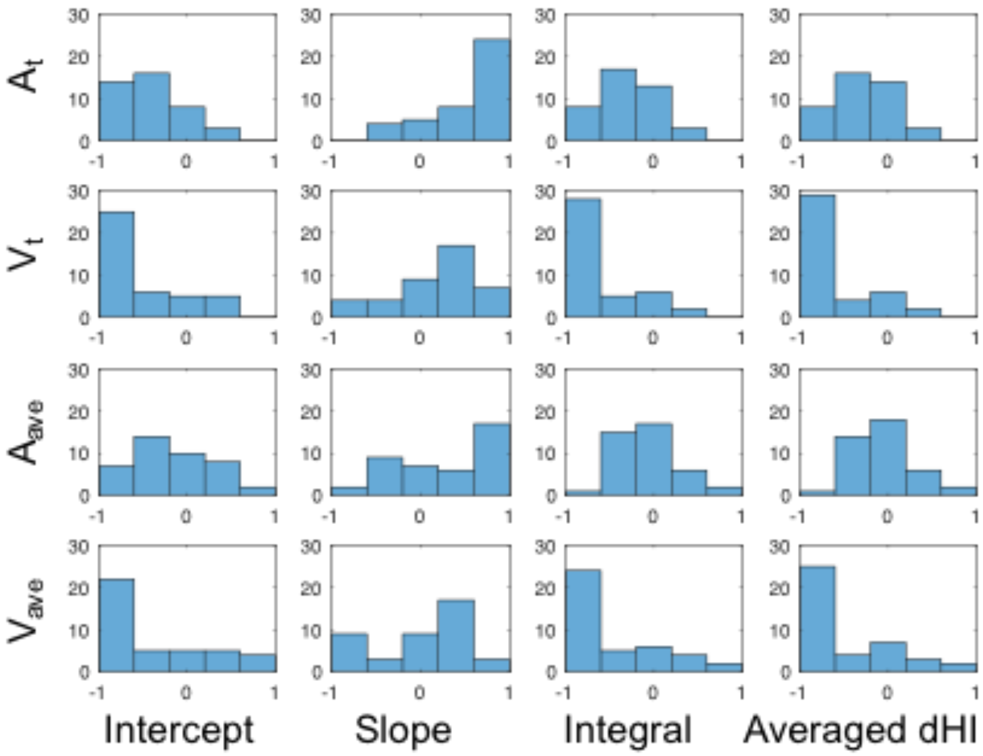

Figure 29–Histograms of correlation coefficients for dHI and fracture parameters.

From these results, some assertions can be made as to which dHI parameters can be used as qualitative predictors of fracturing efficiency. Perhaps the strongest correlation is a negative correlation between the dHI integral and total fracture volume. Intuitively this makes sense; the integral will be larger in a case when dHI does not decrease much over time and therefore has a larger integral. A lack of change in dHI signals that injectivity is not improving, hence smaller fracture volume. Further, the integral will be larger when the initial dHI is high. Anecdotally, stages with high initial dHI values (especially when significantly higher), have low cluster efficiency. Again, this will lead to lower total fracture volumes simply because the fracture count is lower. Graphically both of these scenarios are shown in Figure 30.

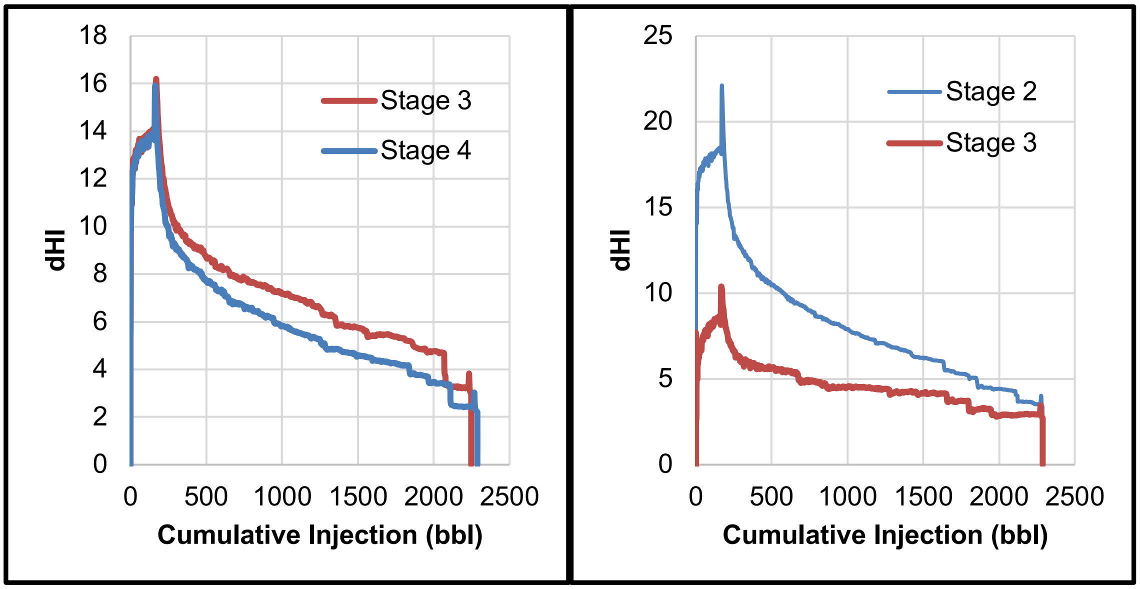

Figure 30–Cases showing graphical behavior of relationship between integral and total fracture volume. The first graph shows a case where injectivity is improved more in Stage 4 than Stage 3 and results in 21% greater fracture volume. The second graph shows a case where Stage 3 has lower cluster efficiency than Stage 2 and results in 24% greater fracture volume.

Another strong correlation is the positive correlation between linear slope and total fracture area. This correlation is somewhat paradoxical, as we would expect more negative slopes to be indicative of more fracture area being created; however, this is not the case. There are two somewhat related behaviors behind this paradoxical correlation. The first is attributed to differing cluster efficiencies. As mentioned above, higher initial dHI values indicate lower cluster efficiency. In order to inject the full stage volume through fewer fractures, injectivity must be increased more relative to a stage with more fractures; hence, a greater slope in dHI. The second reason for this correlation is similar but more nuanced; when one fracture within a stage is being preferentially propagated, the slope will become more negative without increasing total fracture area proportionally. An example of this is shown in Figure 31 where the linear slope of Stage 4 is 6% more negative than that of Stage 3. In this case the standard deviation of fractures created by Stage 4 is 2.5 times greater than the standard deviation of fractures created by Stage 4 resulting in Stage 4 having 13% less total fracture area.

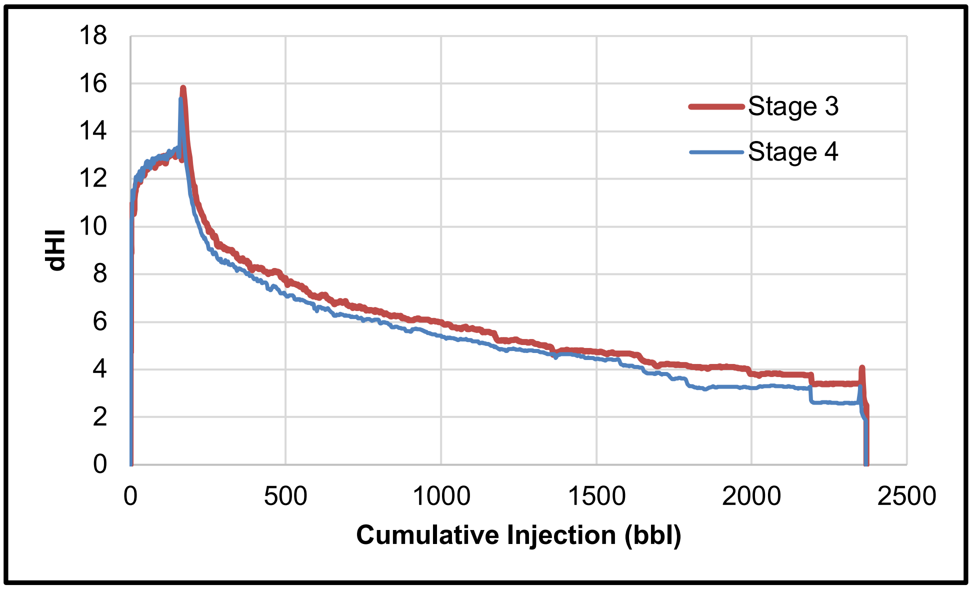

Figure 31–Case showing relationship between slope and total fracture area.

It is important to note that the correlation between averaged dHI and total fracture volume is nearly as good as the correlation first discussed. This is important because it allows the methodology to be applied when only average pressure and rate are available (as is often the case for non-operators) with equal efficacy as shown in

Figure 32. Using the full stage data, we would expect Stages 1 and 3 to have greater fracture volume than Stages 2 and 4. Knowing that there is an inverse relationship between averaged dHI and total fracture volume, we arrive at the same conclusion using the averaged stage data.

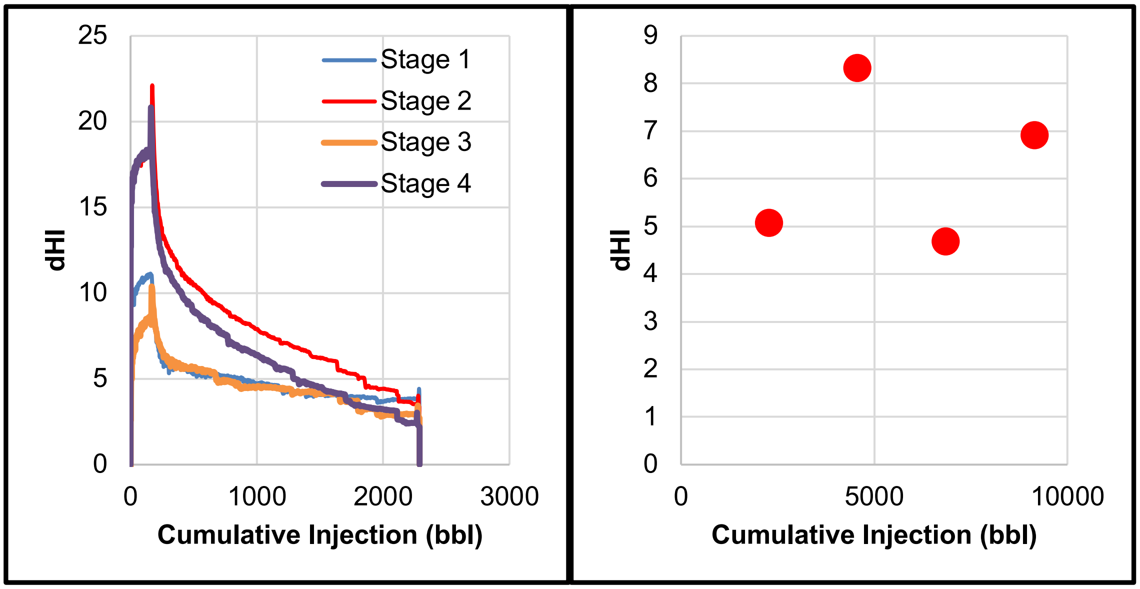

Figure 32–Comparison of full stage data (left) and averaged data (right).

5.4 Sample Well Applications

The results allow high grading of stages along a lateral as shown in Figure 33. When increasing dHI is observed, results from above would indicate that fracturing efficiency is decreasing. Likewise, when decreasing dHI is observed, it can be assumed that fracturing efficiency is improving. In the example below, this approach is used to visually indicate improving and decreasing efficiency from stage to stage along the lateral.

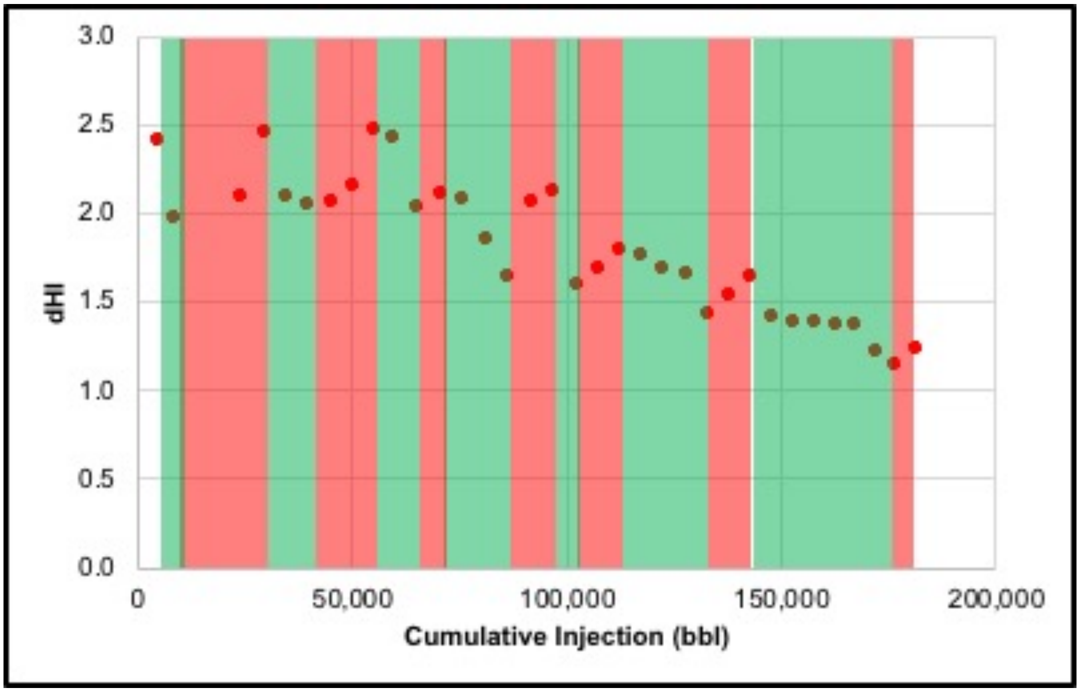

Figure 33–Example of stage high grading within a single completion. Stages with decreasing dHI are shaded green indicating improving fracture efficiency.

Further extrapolating the methodology allows for comparison of fracturing efficiency between separate wells: by plotting dHI for separate wells together and comparing the integrals, we can evaluate which will likely have greater fracture volume. To illustrate this point, Figure 34 shows dHI plots for Well 01 and Well 07 from the Meramec data set. From the RTA results in Chapter 3, total fracture area is computed for reference and confirmation of results expected from the dHI methodology: Well 01 has a total fracture area of 4.6E6 ft^2 and Well 07 has 6.9E6 ft^2. Comparing the integrals of dHI for both wells, the integral of Well 01 is 3% higher than Well 07. This would lead to the conclusion that Well 07 should have greater fracture area, as is the case in the RTA results.

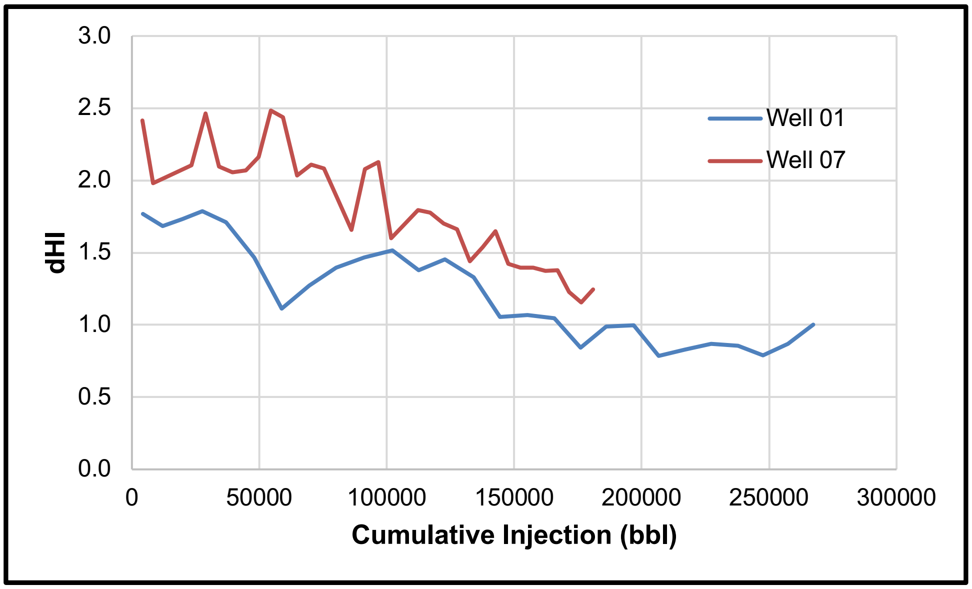

Figure 34–Example of applying methodology to evaluate completion efficiency across two wells. Integral of Well 07 is less than the integral of Well 01.

This chapter has outlined a primary assessment of a new methodology for diagnosis of fracturing efficiency. The new method is quick, is a very simple formulation, and has wide ranging potential. There is certainly room for expanding this initial assessment as there are many parameters that I have not considered within my design of experiments. Further, different experimental designs could generate more granularity in the results and broaden the base of applicability.

Chapter 6: Forecasting Recovery from Meramec

In this chapter, I will present the efforts to history match the available production of approximately ten months. From the result of this match I will make some predictions about some petrophysics, as well as discuss the physics of flow potentially occurring in this well. From there, I will move into forecasting of recovery and try to draw some conclusions as they relate to the recovery to be expected from the Meramec.

6.1 History Matching Initial Production

Beginning with the model at the end of hydraulic fracturing from Chapter 4.1, a simulation case was run in bottomhole pressure control mode. These pressures were calculated in the workflow in Chapter 3 using tubing head pressures and observed rates. From this initial case, a manual history matching process was used to match the production data available. Within this history matching process, a few parameters were used as the primary history matching variables: the exponent ‘a’ from Eq. 3 in Chapter 4.1, the fracture permeability within the SRV, and the relative permeability end-points and Corey exponents. The results of the history match are shown in Figure 35.

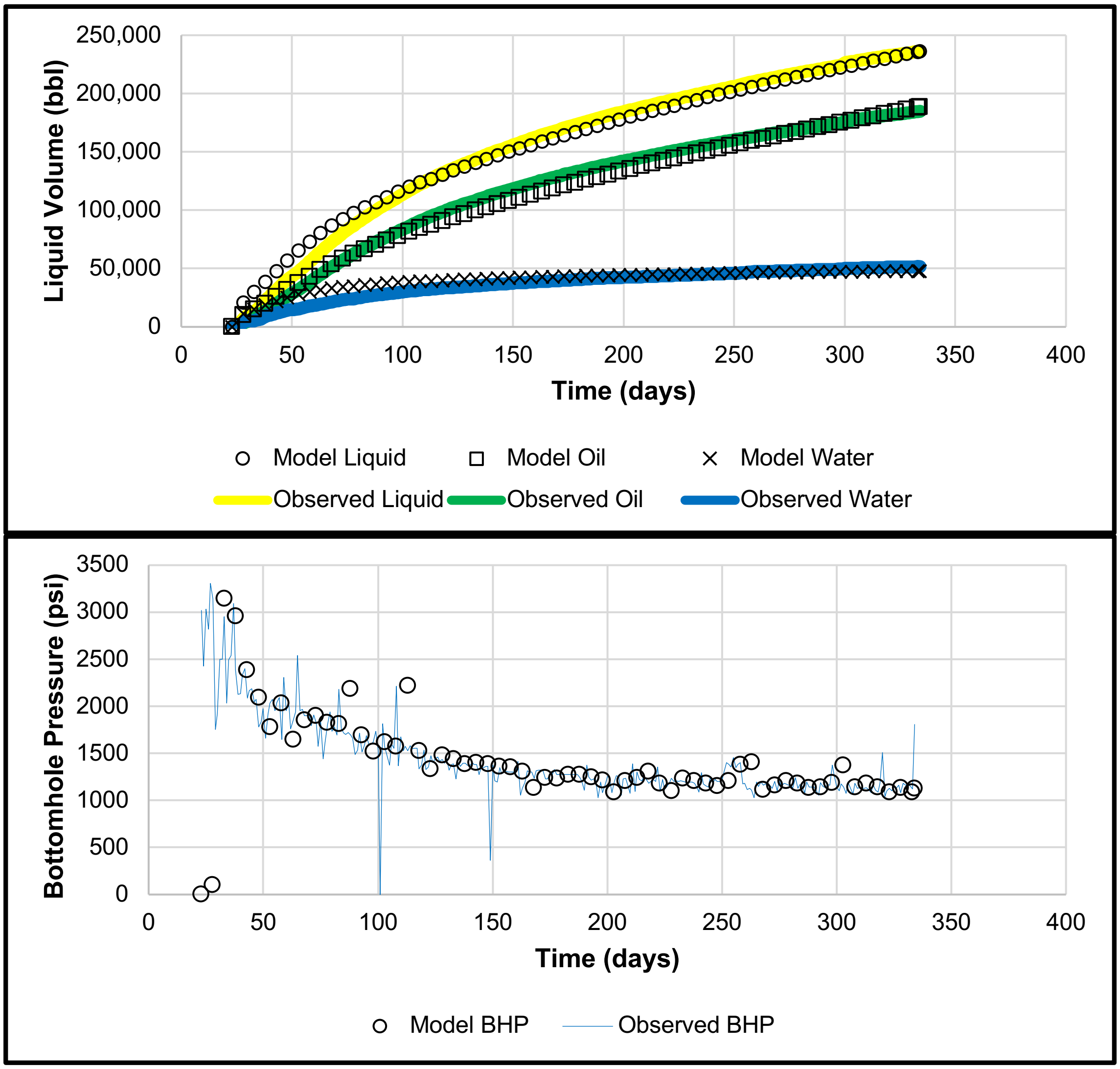

Figure 35–History matched liquid rates and bottomhole pressures.

Matching the evolution of gas-oil ratio over time proved more difficult than matching liquid rates, as evident in the match quality shown in Figure 36. While the gas-oil ratio of the model does begin to increase in a similar manner to the real data, it does so much later. This is likely due to the grid size that I have used. In Jones work on GOR behavior in tight oil reservoirs (2016), he shows that the difference between linear and radial flow has a substantial effect on GOR behavior, with linear flow having increased GOR earlier in the production life of the well. With the grid size I am using (100’ in both the x- and y-direction), I cannot properly model linear flow into a fracture, so I am in effect modeling radial flow, hence the late increase in GOR of my model compared to reality.

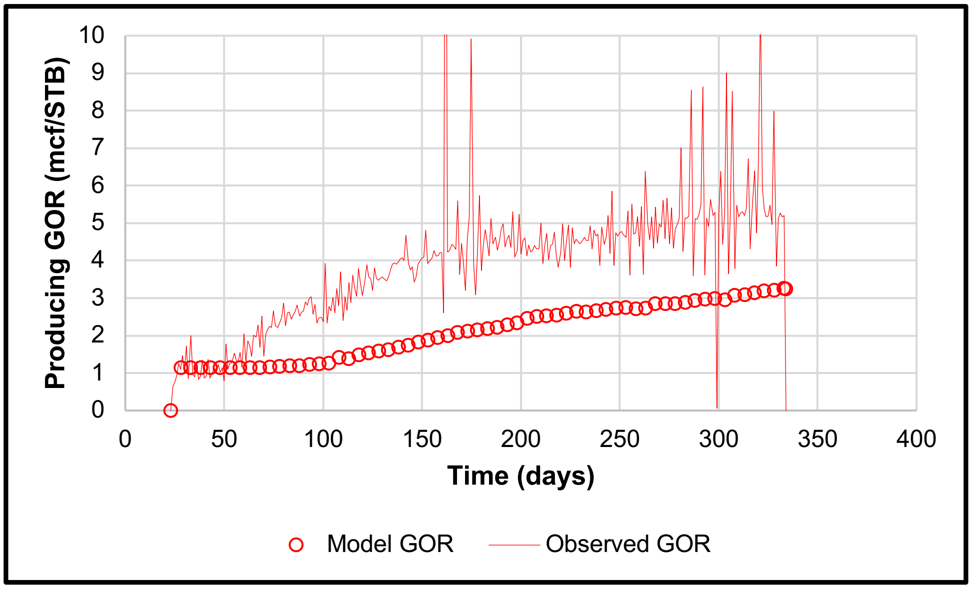

Figure 36–GOR behavior from the model and observed data.

In order to achieve the match above, the 'a' exponent from Eq. 3 was modified from the values in Chapter 4 and found to be 18, 5, and 15 for the x-, y-, and z-directions as applied to the fractures. The mean fracture horizontal permeability before this modification was found to be 2 md. The relative permeability curves for the fractures in this history matched model are shown in Figure 37. As one would expect in a fracture (Diomampo 2001), the Corey exponents are all one and the curves have very low end-point values (zero in most cases).

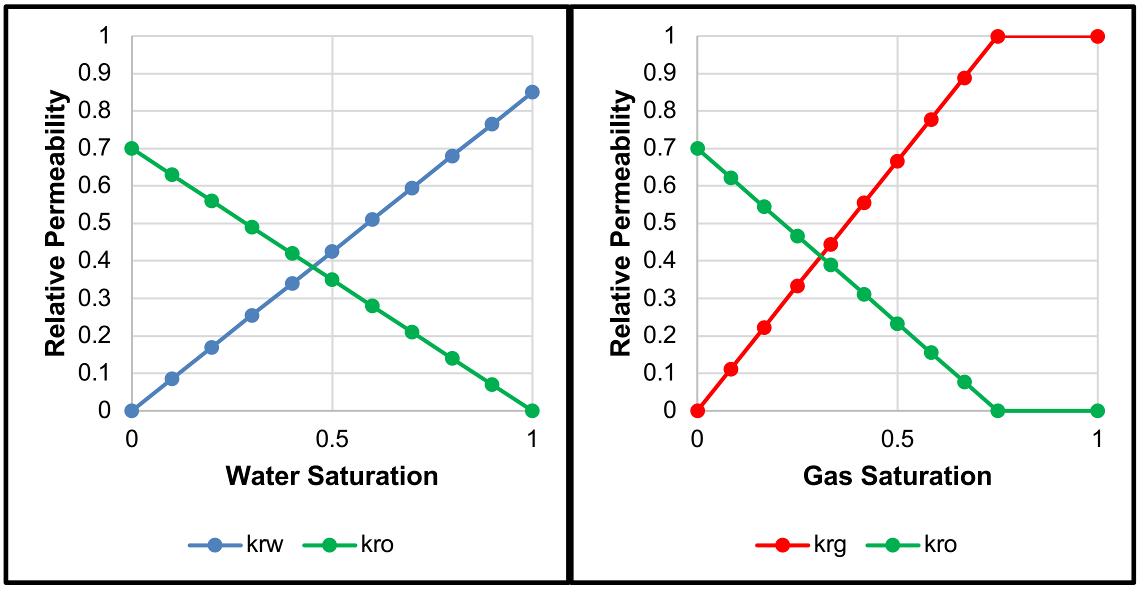

Figure 37–Relative permeability curves in history matched model.

It was found within this history matching process that the methodology I have used for computing the transmissibility multiplier is flawed. This methodology results in very high multipliers below the wellbore, which results in settling of injected water, making matching water production difficult. This could be a flaw in the methodology of scaling based on net stress, or it could be another case where my grid size is too large to capture the physics necessary to properly model the flow within the reservoir.

6.2 Forecasting Forward from Initial Production

Moving forward with this model, a forecasting model was generated. A minimum rate of 20 STB/day is assumed to be the economic limit, and the bottomhole pressure was set to a minimum of 500 psi. With these constraints, cumulative production with time was forecasted and the results are shown in Figure 38. The forecast results in an oil recovery of 447,000 STB and a gas recovery of 2,872 MMSCF. This amounts to an oil recovery factor of 8.6% from the stimulated reservoir volume.

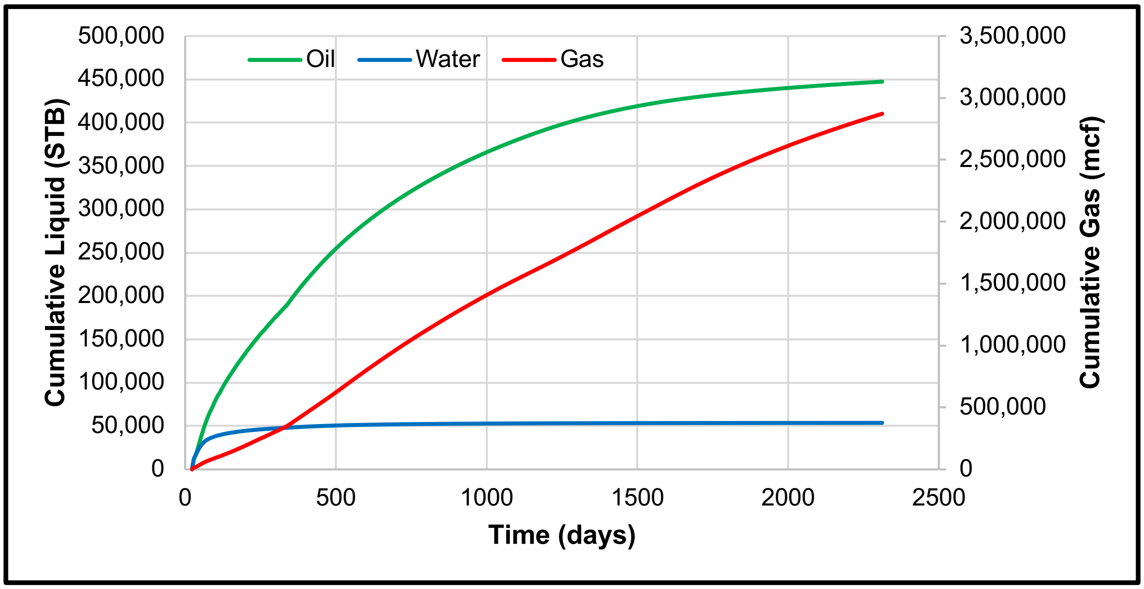

Figure 38–Forecasted cumulative production volumes for oil, gas, and water from Well 07.

Within this chapter approximately ten months of initial production has been history matched. The quality of match relative to liquid volumes is good; however, relative to gas, it seems that the model setup I have used cannot properly capture the flow physics occurring in the reservoir in order to properly match GOR evolution. Nevertheless, with the history matched model, I have forecasted recovery from the well and found an oil recovery factor of 8.6% from the SRV. It should be noted that if one considers the entire field, this recovery factor will over estimate recovery, as due to the irregularities in SRV shapes, the entire reservoir will not likely be stimulated.

Chapter 7: Discussion/Limitations

The iterative workflow presented in Chapter 3 can be used to develop a unified fluid characterization for a regional study and yield a quality match to initial producing fluid behaviors. Further, the workflow simultaneously yields petrophysical and completion results from rate transient analysis that provide crucial information about the reservoir and its development. Most valuable is that this can be completed with relatively little, and often publicly available, data. It is important to note that the workflow provides only an initial characterization. It does not propose any robust history matching or forecasting; the results from the workflow could change as the study moved into dynamic history matching and forecasting.

When the workflow was applied to the study area of the Meramecian interval of the STACK, we obtained the following results:

- Methane molar compositional gradient: 8.2% per 1,000 feet
- Plus-fraction 1 molar compositional gradient: 3.7% per 1,000 feet
- Initial reservoir pressure gradients: 0.42-0.65 psi per 100 feet
- Oil formation volume factor: 1.35-6.50 RB/STB
- Fracture half-length: 540-900 feet
- Fracture height: 200-300 feet
- Well drainage area: 315-505 acres

Further and complete integration of static geologic models will also lead to more complete results and an overall complete reservoir characterization as well as expanding the understanding of the uncertainty in the results. While I have identified secondary evidence of baffles, actually locating and understanding the degree to which the baffles impact the reservoir would require further integration of engineering and geologic studies. Additionally, while the workflow provides a representative fluid and EOS characterization with regard to initial producing fluid properties, it is far from the complete EOS characterization that would be required for complex fluid modeling (such as would be used in enhanced oil recovery modeling).

The single well modeling efforts in Chapter 4 have generated results for the potential size of the SRV surrounding Well 07. The modeling and history matching using a flow simulator has utilized a dual porosity model, with the idea that the fracture component of the dual porosity system represents the induced fracture network from hydraulic fracturing. These results were also compared to modelling results from a finite volume fracture simulator. Results from the flow simulation method indicate a half-length of 550 ft and a height of 260 ft. Results from the fracture simulator show half-length of 350 ft and height of 300 ft. The methodology of using the flow simulator is limited in the fact that it does not explicitly utilize any geomechanical functionality; geomechanics are imposed on the system through the use of rock compaction tables that tabulate pore volume and directional transmissibility modifiers against net stress. While this methodology can certainly capture some of the changes brought on by hydraulic fracturing, it is far from the robustness that would be accomplished with a coupled simulator. Further, as is usually the case, there is further room for improvement in capturing uncertainty. In this work, I have presented one realization that satisfies the observed data, but it is only one of the many thousands of equally plausible realizations that could satisfy the observed data.

The approach to quickly diagnose fracture efficiency presented in Chapter 5 has shown promise in qualitatively evaluating fracture efficiency. Correlations were shown that allow the dHI methodology to indicate qualitative stage by stage differences in total fracture volume and total fracture area from the dHI integral and the dHI slope respectively. Further, averaged integral values along a lateral allow for high grading stages along the lateral, as well as comparison between different wells. With that said, this work is preliminary, and could certainly use a more robust treatment to confirm just how far the methodology can be applied. Efforts were made to encompass many different design parameters so as to have a robust sample size to use to draw conclusions, but there are certainly many more parameters, as well as geologic inputs that would need to be included to have a full treatise of the methodology.

Within Chapter 6, I have history matched production from Well 07 and attained a good match relative to oil and water production. As mentioned previously, the model setup cannot properly capture the GOR evolution, and this is a drawback of the methodology I present in this work. Further, it is a challenge many face when completing simulation studies on tight oil reservoirs. In order to properly capture GOR evolution, there must be granularity in the grid size such that there are several cells between fractures. In a well with a cluster spacing of 35 ft and considering each cluster could correspond with an induced fracture, this would mean cell size along the wellbore would need to be significantly smaller than 35 ft in order to properly capture linear flow into the fractures. Obviously, a model with a cell size this small becomes very computationally burdensome and potentially prohibitive. Further, the methodology I have used to convert net stress into transmissibility multipliers appears to be less than ideal.

Chapter 8: Conclusion

The study in Chapter 3 has presented a workflow that is effective in providing an initial reservoir characterization with use of minimal data and applied it to a study area of the Meramecian interval in the STACK. The workflow allows for development of a unified EOS on a regional scale which provides fluid property distributions. Further, it incorporates the use of rate transient analysis, yielding a characterization of the stimulated near-wellbore region. The integration of these results leads to a characterization that can be utilized in optimization of field development strategies. When applied to our region-scale study of the Meramecian interval, the workflow allowed for interpretation of reservoir pressures across the region. Examining the pressures illuminated the possible presence of baffles in the reservoir. The fluid characterization portion of the workflow allowed for region-wide matching of initial fluid ratios. Rate transient analysis yielded an initial petrophysical characterization and characterization of the near wellbore stimulated region as well as an estimation of the uncertainty in these results.

Chapter 4 presented an estimation of the extent of the SRV of one well in the study area utilizing two different methodologies. First, a history matching process was used utilizing a reservoir flow simulator. Second, a fracture simulator was used, and the results of the two methods were compared. The results varied somewhat, with the sizes from the flow simulator more closely aligning with the RTA results from Chapter 3.

Chapter 5 introduced the use of an adapted formulation of the modified Hall Analysis as an application to diagnose fracture efficiency. It was found that the integral and slope of the dHI plot can be used to qualitatively assess fracture volume and area of a stage relative to other stages in the well. Further, averaged values of dHI integral allow for comparison between completions on different wells. These results potentially have broad reaching applications: quick diagnosis on site during a completion, high grading of stages along a later (potentially allowing for better stage placement), and field wide completion quality evaluations (allowing for better understanding of performance drivers and completion quality mapping).

Chapter 6 used the model from Chapter 4 and history matched production and forecasted recovery for Well 07. From the history matching, mean fracture permeability was found to be 2 md and potential levels of permeability enhancement around the wellbore were found. From forecasting, ultimate oil recovery was found to be 447,000 STB with an oil recovery factor of 8.6% from the stimulated reservoir volume.

References

Abdallah, L. A. 2016. The Geochemical Characterization of Oil Samples from the Mississippian Meramec Formation in Eastern Anadarko Basin, Oklahoma. MS Thesis, University of Tulsa, Tulsa, Oklahoma (2016).

Agarwal, R. G., Gardner, D. C., and Kleinsteiber, S. W. 1998. Analyzing Well Production Data Using Combined Type Curve and Decline Curve Analysis Concepts. Presented at the SPE Annual Technical Conference and Exhibition, New Orleans, Louisiana, 27-30 September. SPE-49222-MS. https://doi.org/10.2118/49222-MS.

Akai, T., Takakuwa, Y., and Sato, K. 2016. Pressure Dependent Permeability of Tight Rocks. Presented at the SPE Low Perm Symposium, Denver, Colorado, 5-6 May. SPE-180262-MS. https://doi.org/10.2118/180262-MS.

Alt II, R. C., and Zoback, M. D. 2017. In Situ Stress and Active Faulting in Oklahoma. Bulletin of the Seismological Society of America, 107(1). http://dx.doi.org/10.1785/0120160156.

Ball, M. M., Henry, M. E., & Frezon, S. E. (1991). Petroleum geology of the Anadarko basin region, Province (115), Kansas, Oklahoma, and Texas (No. 88-450-W). US Geological Survey.

Bhandari, A. R., Flemings, P. B., Polito, P. J, et al. 2015. Anisotropy and Stress Dependence of Permeability in the Barnett Shale. Transport in Porous Media 108 (2): 393-411. http://dx.doi.org/10.1007/s11242-015-0501-1.

Chin, L. Y., Raghavan, R., and Thomas, L. K. 2000. Fully Coupled Geomechanic and Fluid-Flow Analysis of Well with Stress-Dependent Permeability. SPE Journal 5 (1): 32-45. SPE-58968-PA. https://doi.org/10.2118/58968-PA.

Dean, R. H., and Schmidt, J. H. 2008. Hydraulic Fracture Predictions with a Fully Coupled Geomechanical Reservoir Simulator. Presented at the SPE Annual Technical Conference and Exhibition, Denver, Colorado, 21-24 September. SPE-116470-MS. https://doi.org/10.2118/116470-MS.

Diomampo, G. P. 2001. Relative Permeability Through Fractures. SGP-TR-170, Stanford University, Stanford, California (August 2001).

Fekete. 2018. Surveillance Analysis Theory. *Fekete,* http://www.fekete.com/SAN/WebHelp/FeketeHarmony/Harmony_WebHelp/Content/HTML_Files/Reference_Material/Analysis_Method_Theory/Surveillance_Theory.htm (access 25 April 2018).

Flinton, K. C. 2016. The Effects of High-Frequency Cyclicity on Reservoir Characteristics of the “Mississippian Limestone”, Anadarko Basin, Kingfisher

County, Oklahoma. BS Thesis, Oklahoma State University, Stillwater, Oklahoma (May 2012).

Izgec, B., Kabir, C. S. 2009. Real-Time Performance Analysis of Water-Injection Wells. SPE Res Eval & Eng 12 (1): 116-23. SPE-109876-PA. https://doi.org/10.2118/109876-PA.

Ji, L., Settari, A. and Sullivan, R. B. 2009. A Novel Hydraulic Fracturing Model Fully Coupled with Geomechanics and Reservoir Simulation. SPE Journal 14 (3): 423-430. SPE-110845-PA. https://doi.org/10.2118/110845-PA.

Jones, R. S. 2016. Producing-Gas/Oil-Ratio Behavior of Multifractured Horizontal Wells in Tight Oil Reservoirs. SPE Res Eval & Eng 19 (3): 1-13. SPE-184397-PA. https://doi.org/10.2118/184397-PA.

Jones, R. S., Pownall, B., and Franke, J. 2014. Estimating Reservoir Pressure from Early Flowback Data. Presented at the Unconventional Resources Technology Conference, Denver, Colorado, 25-27 August. URTEC-1934785-MS. https://doi.org/10.15530/URTEC-2014-1934785.

Karacaer, C., Thompson, L., and Firincioglu, T. 2015. Unraveling Minimum Liquid Yields from Variable PVT and Production Data in the Woodford using EOS. Presented at the Unconventional Resources Technology Conference, San Antonio, Texas, 20-22 July. URTEC-2154623-MS. https://doi.org/10.15530/URTEC-2015-2154623.

Katsuki, D., Gutierrez, M., and Tutuncu, A. N. 2013. Laboratory Determination of the Continuous Stress-Dependent Permeability of Unconventional Oil Reservoir Rocks. Presented at the Unconventional Resources Technology Conference, Denver, Colorado, 12-14 August. SPE-168912-MS.

Kornacki, A. S., and Dahl, J. E. 2016. Evidence Some Oil Accumulations in the Woodford Formation and the Meramec Formation Received an Additional Charge of Very Dry Thermal Gas. Presented at the AAPG 2016 Annual Convention and Exhibition, Calgary, Alberta, 19-22 June.

Mazzullo, S. J., B. W. Wilhite, D. R. Boardman, B. T. Morris., and C. J. Godwin, 2016, Stratigraphic architecture and petroleum reservoirs in lower to middle mississippian strata (Kinderhookian to basal Meramecian) in subsurface central to southern Kansas and northern Oklahoma: Shale Shaker, vol. 67 no. 2, p. 20-49.

Oklahoma Corporation Commission. 2017. Oil and Gas Info. Occeweb, https://apps.occeweb.com/RBDMSWeb_OK/OCCOGOnline.aspx (accessed 10 May 2017).

Palacio, J. C., and Blasingame, T. A. 1993. Decline-Curve Analysis with Type Curves – Analysis of Gas Well Production Data. Presented at the Low Permeability

Reservoirs Symposium, Denver, Colorado, 26-28 April. SPE-25909-MS. https://doi.org/10.2118/25909-MS.

Peng, D., and Robinson, D. B. 1976. A New Two-Constant Equation of State. Industrial & Engineering Chemical Fundamentals. 15 (1): 59-64. http://dx.doi.org/10.1021/i160057a011.

Price, B., Pollack, A., Lamb, A. 2017. Depositional Interpretation and Sequence Stratigraphic Control on Reservoir Quality and Distribution in the Meramec STACK Play: Anadarko Basin. Presented at the AAPG Annual Convention and Exhibition, Houston, Texas, 4 April.

Senters, C. W., Van Sickle, S. and Snyder, D., 2016. Evaluation of Completion Practices in the STACK Using Completion Diagnostics and Production Analysis. presentation at the SPE Annual Technical Conference and Exhibition held in Dubai, UAE, 26-28 September. SPE-181441-MS. https://doi.org/10.2118/181441-MS.

Uzun, I., Kurtoglu, B., and Kazemi, H. 2016. Multiphase Rate-Transient Analysis in Unconventional Reservoirs: Theory and Application. SPE Res Eval & Eng 19 (4): 553-556. SPE-171657-PA. https://doi.org/10.2118/171657-PA.

Welker, C., Feiner, S., and Lishansky, R., et al. 2016. Trapped Fluid Analysis of 58 Wells from the SCOOP and STACK Plays, Oklahoma. Presented at the Unconventional Resources Technology Conference, San Antonio, Texas, 1-3 August. URTEC-2461587-MS. https://doi.org/10.15530/URTEC-2016-2461587.

Whitson, C. H., and Sunjerga, S. 2012. PVT in Liquid-Rich Shale Reservoirs. Presented at the SPE Annual Technical Conference and Exhibition, San Antonio, Texas, 8-10 October. SPE-155499-MS. https://doi.org/10.2118/155499-MS.